2013

Modeling Terrestrial Gamma Ray Flashes Produced By Relativistic Feedback Discharges

Ningyu Liu

Joseph R. Dwyer

JOURNAL OF GEOPHYSICAL RESEARCH: SPACE PHYSICS, VOL. 118, 2359–2376, doi:10.1002/jgra.50232, 2013

Modeling terrestrial gamma ray flashes produced by relativistic feedback discharges

Ningyu Liu[1] and Joseph R. Dwyer[1]

Received 5 December 2012; revised 12 March 2013; accepted 13 March 2013; published 3 May 2013.

[1] This paper reports a modeling study of terrestrial gamma ray flashes (TGFs) produced by relativistic feedback discharges. Terrestrial gamma ray flashes are intense energetic radiation originating from the Earth's atmosphere that has been observed by spacecraft. They are produced by bremsstrahlung interactions of energetic electrons, known as runaway electrons, with air atoms. An efficient physical mechanism for producing large fluxes of the runaway electrons to make the TGFs is the relativistic feedback discharge, where seed runaway electrons are generated by positrons and X-rays, products of the discharge itself. Once the relativistic feedback discharge becomes self-sustaining, an exponentially increasing number of relativistic electron avalanches propagate through the same high-field region inside the thundercloud until the electric field is partially discharged by the ionization created by the discharge. The modeling results indicate that the durations of the TGF pulses produced by the relativistic feedback discharge vary from tens of microseconds to several milliseconds, encompassing all durations of the TGFs observed so far. In addition, when a sufficiently large potential difference is available in thunderclouds, a self-propagating discharge known as the relativistic feedback streamer can be formed, which propagates like a conventional positive streamer. For the relativistic feedback streamer, the positive feedback mechanism of runaway electron production by the positrons and X-rays plays a similar role as the photoionization for the conventional positive streamer. The simulation results of the relativistic feedback streamer show that a sequence of TGF pulses with varying durations can be produced by the streamer. The relativistic streamer may initially propagate with a pulsed manner and turn into a continuous propagation mode at a later stage. Milliseconds long TGF pulses can be produced by the feedback streamer during its continuous propagation. However, the continuous propagation of the streamer tends to be unstable, because it does not expand like the conventional positive streamer. Its head electric field continues to increase and can reach half of the conventional breakdown threshold field, which results in an ion density of $3–10 \times 10^{14}$ m^{-3} in the channel immediately following the head. The spatial width of the high field region in the streamer head is about 100 m and the streamer speed is about 5×10^5 m/s. As a result, conventional positive streamers can be initiated from thundercloud hydrometeors or inhomogeneities of enhanced conductivities of millimeter sizes in the relativistic feedback streamer head and the positive streamers may further result in the formation of leaders. In addition, a relativistic feedback streamer can result in a charge moment change of several tens of coulomb-kilometers in a few tens of milliseconds, indicating that the relativistic feedback discharge process could be an important component for thundercloud charge dynamics.

Citation: Liu, N. Y., and J. R. Dwyer (2013), Modeling terrestrial gamma ray flashes produced by relativistic feedback discharges, *J. Geophys. Res. Space Physics*, *118*, 2359–2376, doi:10.1002/jgra.50232.

1. Introduction

[2] Terrestrial gamma ray flashes (TGFs) are brief bursts (typically <1 ms) of multi-MeV radiation originating from thunderclouds in the Earth's atmosphere. They were first detected by the Burst and Transient Source Experiment (BATSE) aboard the Compton Gamma Ray Observatory (CGRO) [*Fishman et al*. 1994] and have since been measured by several spacecraft, including Reuven Ramaty High

[1]Geospace Physics Laboratory, Department of Physics and Space Sciences, Florida Institute of Technology, Melbourne, Florida, USA.

Corresponding author: N. Y. Liu, Department of Physics and Space Sciences, Florida Institute of Technology, Melbourne, FL 32901, USA. (nliu@fit.edu)

2169-9380/13/10.1002/jgra.50232

Energy Solar Spectroscopic Imager (RHESSI) [*Smith et al.*, 2005; *Grefenstette et al.*, 2009], Astro-rivelatore Gamma a Immagini Leggero (AGILE) [*Marisaldi et al.*, 2010; *Tavani et al.*, 2011], and Fermi [*Briggs et al.*, 2010, *Connaughton et al.*, 2010; *Fishman et al.*, 2011]. The confirmed maximum energies of individual photons of the TGFs are about 40 MeV [*Marisaldi et al.*, 2010; *Briggs et al.*, 2010], although photons with energies up to 100 MeV were also reported by AGILE [*Tavani et al*. 2011]. According to spectral analysis of the TGFs (as well as the analysis of TGF-associated sferics; see below) [*Dwyer and Smith*, 2005; *Carlson et al.*, 2007], they are produced inside and/or immediately above thunderclouds by bremsstrahlung interactions of energetic electrons known as runaway electrons with air atoms. As the gamma rays travel through the atmosphere, they can produce, via Compton scattering and pair production, energetic electrons and positrons that when produced above about 40 km altitude, are able to escape the atmosphere as well. The escaped electrons and positrons propagate along the Earth's magnetic field lines and may be detected by a spacecraft when it crosses their trajectory [*Dwyer et al.*, 2008; *Carlson et al.*, 2009; *Cohen et al.*, 2010a; *Briggs et al.*, 2011]. The detected pulses of the electron and positron beams last about a few tens of milliseconds, much longer than the normal TGFs, but have a smaller average energy per particle. A comprehensive review of many aspects of the TGFs is available in *Dwyer et al.* [2012].

[3] Since the discovery of the TGFs, lightning radio measurements have revealed the connections between the TGFs and the lightning discharges [e.g., *Inan et al.*, 1996; *Cummer et al.*, 2005; *Stanley et al.*, 2006; *Cohen et al.*, 2006; *Cohen et al.*, 2010b; *Shao et al.*, 2010; *Lu et al.*, 2010, 2011; *Connaughton et al.*, 2010; *Cummer et al.*, 2011]. Detailed analysis of measurements of lightning sferics associated with a dozen of RHESSI TGFs found that the TGF events were closely correlated with positive in-cloud (+IC) lightning discharge activities detected by the Los Alamos Sferic Array [*Stanley et al.*, 2006; *Shao et al.*, 2010]. Close correlations between more RHESSI TGF events and lightning ELF/VLF sferics were later reported by *Cohen et al*. [2010b] with the Stanford AWESOME instrument. A more detailed picture of the TGF and IC relationship was drawn by an analysis of broadband lightning sferics and a RHESSI TGF event [*Lu et al.*, 2010]. According to this work, the TGF event occurred during the initial +IC lightning leader development in which a slow discharge process produced an unusually large charge moment change (90 C km) in a few milliseconds, and several isolated fast discharge processes of 10–20 μs time scales were superimposed on this slow process. With better timing accuracy of Fermi TGFs, Lightning discharge processes were detected by the World Wide Lightning Location Network within tens of microseconds of the peak of the Fermi TGFs [*Connaughton et al.*, 2010]. This result was later confirmed by the work of *Cummer et al.* [2011], who further suggested, however, that there may not be a causative relationship between the fast processes (10–20 μs) and the TGFs. Their analysis of two Fermi TGF events showed that the timing, duration, and intensity variation of the TGF event match a slower discharge process of 50–100 μs time scales, suggesting the currents that produce the RF emissions are closely related to the production of the TGF. *Dwyer* [2012] modeled the currents produced by the energetic electron and resulting ionization and suggested that the radio pulses observed in association with the TGF were from the TGF itself and not lightning.

[4] Terrestrial gamma ray flashes are produced by bremsstrahlung interactions of runaway electrons with air atoms. The idea of electron runaway phenomena in thundercloud fields was first proposed by *Wilson* [1925], who recognized that energetic electrons can gain energy in thundercloud electric fields with a rate faster than that of energy loss in ionizing air molecules, and they can accelerate to relativistic speeds and produce gamma radiation. The energetic electrons can be seeded by radioactive decays or cosmic rays. *Gurevich et al.* [1992] introduced the Relativistic Runaway Electron Avalanche (RREA) mechanism that suggests when Møller scattering (electron-electron elastic scattering) is included, the runaway electrons described by Wilson will undergo avalanche multiplication, resulting in a large number of relativistic runaway electrons for each energetic seed electron injected into the high-field region in thunderclouds. The threshold electric field of the RREAs, E_{th}, was later determined by numerical simulations to be about 2.84×10^5 V/m $\times n$, where n is the density of air with respect to that at sea level [*Symbalisty et al.*, 1998; *Dwyer*, 2003]. This threshold field is near the maximum electric field strength measured inside thunderclouds [e.g., *Stolzenburg et al.*, 2007], suggesting runaway electron avalanches may be common inside thunderclouds. Monte Carlo simulations on the RREAs from different research groups have consistently shown that the avalanche length λ of the RREAs is approximately 7.3 MV/($E - E_d \times n$), where E is the electric field and $E_d = 2.76 \times 10^5$ V/m [*Dwyer*, 2012]. Its value at thundercloud altitudes is about hundreds of meters down to tens of meters when the field is slightly above the threshold field E_{th} or a few times larger, respectively. After the RREAs go through a distance of several avalanche lengths, the energy spectrum of the runaway electrons reaches steady state and takes a form of exp(–ε/7.3 MeV), where ε is the energy of the runaway electrons. This is because the force on a runaway electron is nearly unvarying with its energy while the total number of the runaway electrons exponentially increases with an e-folding length λ. However, it was later found that the relativistic electron avalanches acting on the cosmic rays alone could not generate enough numbers of energetic photons to make the observed TGFs [*Dwyer*, 2008].

[5] There are currently two theories under consideration for TGF production in thunderclouds. The first theory is based on the cold runaway (also known as thermal runaway or high-field runaway) mechanism advanced by *Gurevich* [1961]. When the electric field is increased above a critical field, which is about 100 times the RREA threshold field, all free electrons may run away and in particular, the thermal population created at low energies may run away. Simulation results based on the Monte Carlo model [*Moss et al.*, 2006; *Celestin and Pasko*, 2011; *Celestin et al.*, 2012], particle-in-cell method with Monte Carlo collision [*Chanrion and Neubert*, 2008, 2010], and hybrid approach combining both particle and fluid descriptions [*Li et al.*, 2008] show that the runaway electrons can be produced by conventional streamers propagating in strong electric fields,

which may occur during the corona flash stage of negative lightning leader stepping [*Moss et al.*, 2006; *Celestin and Pasko*, 2011; *Celestin et al.*, 2012]. Observations of X-rays from lightning leaders [*Moore et al.*, 2001; *Dwyer et al.*, 2003] and spark discharges [*Dwyer et al*. 2005] provide support for this theory. This process may produce large enough seed runaway electron fluxes that further go through avalanche multiplication in thundercloud fields and make TGFs [*Dwyer*, 2008; *Dwyer et al.*, 2010].

[6] The other theory is RREAs augmented by the relativistic positive feedback mechanism introduced by *Dwyer* [2003], and the resulting discharge is termed as the relativistic feedback discharge [*Dwyer*, 2012]. Due to the positive feedback mechanism, relativistic runaway electron avalanches of increasing strength repeatedly go through a strong thundercloud electric field region and are able to generate large fluxes of gamma photons in tens to hundreds of microseconds. A recent comprehensive modeling study of the TGFs with the relativistic feedback discharge mechanism has successfully reproduced many observed TGF aspects, including the time structures, intensities, and associated current moments [*Dwyer*, 2012].

[7] The purpose of this paper is to report a new modeling study on the TGFs and relativistic feedback discharges following Dwyer's work. A new computer code, independent from the one used in *Dwyer* [2012], was developed for this purpose. The code is built on a plasma discharge code that has been used for studying conventional streamer discharges in sprites, lightning and laboratory experiments [e.g., *Liu and Pasko*, 2004; *Liu et al.*, 2009a, 2009b; *Liu*, 2010; *Liu et al.*, 2012], and sprite halos [*Liu*, 2012]. The components for modeling the relativistic feedback discharge and the production of energetic photons have been added. In contrast to the work of *Dwyer* [2012], the new code can fully model transport of low-energy electrons and ions, and their source and loss processes. It also uses different numerical approaches to solve the relativistic discharge model equations. However, simulation results presented below show that the main properties of the relativistic feedback discharge and the gamma rays produced are very similar, confirming the conclusions drawn in *Dwyer* [2012] that the intense gamma ray flashes can be produced naturally by the relativistic feedback discharge developing in large-scale thundercloud and lightning fields. In addition, the new simulation results show that the relativistic discharge can also generate millisecond long gamma ray pulses and that the propagation of the relativistic feedback streamer, a self-propagating discharge resulting from the relativistic feedback discharge mechanism, tends to be unstable. The head field of the relativistic feedback streamer can reach half of the conventional breakdown threshold field, which makes initiation of conventional streamers and leaders from thundercloud hydrometeors or localized conductivity enhancements possible according to recent modeling results on streamers [*Liu*, 2010; *Liu et al.*, 2012; *Kosar et al.*, 2012] and streamer-to-leader transitions [*Riousset et al.,* 2010; *da Silva and Pasko,* 2012].

2. Model Formulation

[8] The basic idea of the relativistic feedback discharge (RFD) mechanism is that the positrons and the X-ray photons generated by the runaway electron avalanches can produce seed runaway electrons at the beginning of the avalanche region initiating secondary runaway electron avalanches [*Dwyer*, 2003, 2012]. When runaway electrons move across a high-field ($> E_{\text{th}}$) region inside thunderclouds, positrons and X-ray photons are produced. The positrons can turn around and run away in the opposite direction of the avalanche and reach the start of the avalanche region, where they can make seed runaway electrons via hard elastic scattering (Bhahba scattering) with atomic electrons in air. Similarly, the X-ray photons can Compton backscatter to the beginning of the avalanche region and produce seed runaway electrons via either Compton scattering or photoelectric absorption. The produced runaway electrons then seed secondary avalanches that go through the same high field region and produce positrons and X-ray photons, and so on. The above processes repeat until the thundercloud high-field region is partially discharged by the ionization created by the discharge. Note that in this paper, we refer to the energetic radiation leading to the feedback as X-rays, it may as well be called gamma rays according to the convention used in space physics (gamma rays for photons with energies greater than ~100 keV) because emissions up to tens of MeV are produced. However, since the processes responsible for the photon feedback mechanisms also work with photons having energies smaller than 100 keV, it is more inclusive to call the feedback mechanism as the X-ray feedback, in the broad sense that X-rays are the energetic radiation produced from atomic transitions.

[9] If there is a sufficient potential difference across the avalanche region, large numbers of positrons and X-ray photons are produced during each generation that can produce more seed runaway electrons than the previous generation. As a result, the avalanches strengthen after each cycle. Two parameters are useful to describe this feedback process: the feedback factor γ and the feedback cycle time τ_{fb}. The feedback time τ_{fb} is the average time for the runaway electrons and the backward propagating positrons (or X-rays) to complete one roundtrip within the avalanche region, and γ is the fractional increase or decrease in the number of the runaway electrons during each cycle. For the discharge driven by the relativistic feedback mechanism, the total numbers of the runaway particles therefore vary with time t as $\propto \gamma^{t/\tau_{fb}} = \exp(t/\tau')$, i.e., the total numbers of the particles change exponentially in time with an e-folding time $\tau' = \tau_{fb}/\ln(\gamma)$.

2.1. Energetic Particle Transport

[10] According to *Dwyer* [2012], the transport equation for the runaway electrons or the positrons is

$$\frac{\partial n_r}{\partial t} + \nabla \cdot (\vec{v} n_r) - \nabla \cdot (\hat{D} \nabla n_r) - \frac{n_r}{\tau} = S, \tag{1}$$

where n_r is either the runaway electron (n_{re}) or the positron (n_{rp}) density, $\vec{v}$ is the average velocity of the runaway electrons or the positrons, $\hat{D}$ is the diffusion coefficient tensor, τ is the relativistic avalanche time for the runaway electrons or the annihilation time (having a negative value) for the positrons, and S is the source from either cosmic rays or the relativistic feedback. To model the relativistic feedback

discharge, a solution driven by a source $S(\vec{x},t) = S_0(\vec{x})\exp(t/\tau')$ is sought, so $n_r(\vec{x},t) = n_0(\vec{x})\exp(t/\tau')$. The transport equation then becomes

$$\nabla\cdot(\vec{v}n_r) - \nabla\cdot(\hat{D}\nabla n_r) - \frac{n_r}{\tau_t} = S,\quad \frac{1}{\tau_t} = \frac{1}{\tau} - \frac{1}{\tau'}, \tag{2}$$

which is the equation to be solved for the runaway electron density or the positron density. The average velocity $\vec{v}$ of the runaway electrons and the positrons is $-0.89c\times\vec{E}/E$ and $c\times\vec{E}/E$, respectively, where c is the speed of light and $\vec{E}/E$ gives the unit vector pointing in the direction of $\vec{E}$. For a detailed description of the model equation, the reader is referred to the paper by *Dwyer* [2012]. Below, we focus on describing the aspects of the present study that are different from that work.

[11] The diffusion coefficient tensor $\hat{D}$ was found in *Dwyer* [2010] in terms of the lateral and longitudinal diffusion coefficients referenced to the field direction. Assuming cylindrical symmetry, let u and v be the curvilinear coordinates of the coordinate system consisting of the electric field lines and the equipotentials, and the diffusion tensor is

$$\hat{D} = \begin{bmatrix} D^{uu} & 0 \\ 0 & D^{vv} \end{bmatrix}.$$

Dwyer [2012] used such a coordinate system to numerically solve equation (2), which has great advantages in obtaining accurate and stable numerical results because there are no cross-diffusion terms in the transport equation [*Albert and Young*, 2005]. However, the implementation of the method is not easy, particularly because several other equations (see below) are solved when modeling the RFD so that several different numerical grids could be present during the simulation. For the current study, we decide to use a fixed numerical grid to discretize equation (2), and it is therefore necessary to transform $\hat{D}$ to the cylindrical coordinate system. A straightforward transformation is formulated as follows. At any point (r,z) in the 2-D cross section of the system, the field line coordinate system can be found by rotating the cylindrical system by the angle ϕ subtended by the field direction and the radial direction. So for any vector $\vec{A}$,

$$\begin{bmatrix} A_u \\ A_v \end{bmatrix} = \begin{bmatrix} \cos\phi & \sin\phi \\ -\sin\phi & \cos\phi \end{bmatrix}\begin{bmatrix} A_r \\ A_z \end{bmatrix}, \tag{3}$$

and

$$\begin{bmatrix} A_r \\ A_z \end{bmatrix} = \begin{bmatrix} \cos\phi & -\sin\phi \\ \sin\phi & \cos\phi \end{bmatrix}\begin{bmatrix} A_u \\ A_v \end{bmatrix}, \tag{4}$$

where $\cos\phi = E_r/E$ and $\sin\phi = E_z/E$. The diffusion flux $\hat{D}\nabla n_r$ and the density gradient ∇n_r in equation (2) are both expressed in the field line system. To obtain the diffusion flux expression in the cylindrical system, $\hat{D}\nabla n_r$ needs to be transformed using equation (4), while ∇n_r found in the cylindrical system needs to be converted to the field line system. Therefore, the diffusion tensor $\hat{D}_c$ in the cylindrical system is

$$\hat{D}_c = \begin{bmatrix} \cos\phi & -\sin\phi \\ \sin\phi & \cos\phi \end{bmatrix}\begin{bmatrix} D^{uu} & 0 \\ 0 & D^{vv} \end{bmatrix}\begin{bmatrix} \cos\phi & \sin\phi \\ -\sin\phi & \cos\phi \end{bmatrix} = \begin{bmatrix} D^{rr} & D^{rz} \\ D^{zr} & D^{zz} \end{bmatrix}.$$

Now, the cross-diffusion terms of $\hat{D}_c$ in general are nonzero, which could pose a challenge for numerical simulations. In addition, $\hat{D}_c$ depends on the direction of the electric field and needs to be calculated when the electric field is changed.

[12] The positrons are produced by pair production of MeV gamma rays emitted by the runaway electrons. Knowing the runaway electron density at t, the positron source function S_p, the production rate of the positrons at location $\vec{x}$ due to the runaway electrons at $\vec{x}'$, at a future time $t+\Delta t$ is calculated as

$$S_p(\vec{x},t+\Delta t) = \mathrm{eff}_p(\vec{x})\int vn_{re}(\vec{x}',t)\,\exp\left(\frac{\Delta t}{\tau'} - \frac{|z-z'|}{v\tau'}\right) n_{p0}(\vec{x},\vec{x}')\mathrm{d}V'. \tag{5}$$

[13] The symbol eff_p represents the efficiency for the positrons to turn around and run away, and it is a function of local reduced electric field E/n and therefore depends on the location $\vec{x}$. The term $\exp(\Delta t/\tau' - |z-z'|/v\tau')$ accounts for the change of the runaway electron density with time and the propagation delays from the runaway electrons at the source location $\vec{x}'$ to $\vec{x}$. The term $n_{p0}(\vec{x},\vec{x}')$ characterizes the averaged positron density distribution produced by a runaway electron traversing 1 m along the avalanche direction. Note that the radial distance in equation (11) to calculate n_{p0} given in *Dwyer* [2012] should have been written as $r = \sqrt{(x-x')^2 + (y-y')^2}$. If S_p is known, equation (2) can be solved for the positron density n_{rp}. Knowing n_{rp}, the electron source function from Bhahba scattering, i.e., production of the runaway electrons due to the positron feedback, is

$$n_s(\vec{x},t) = \mathrm{eff}_{re}(\vec{x})cn_{rp}(\vec{x},t)/\lambda(\vec{x}),$$

where the function eff_{re} describes the efficiency, relative to that of the runaway electrons, of producing new seed particles, and $\lambda(\vec{x})$ is the e-folding length of the relativistic runaway electron avalanches.

[14] The electron source function due to X-ray feedback is described by an equation similar to (5)

$$S_x(\vec{x},t+\Delta t) = \mathrm{eff}_x(\vec{x})\int vn_{re}(\vec{x}',t)\,\exp\left(\frac{\Delta t}{\tau'} - \frac{|z-z'|}{v\tau'}\right) n_{x0}(\vec{x},\vec{x}')\mathrm{d}V', \tag{6}$$

where eff_x is the efficiency of each initial runaway electron, traversing 1 m along the avalanche direction, creating secondary seed runaway electrons via X-rays, and $n_{x0}(\vec{x},\vec{x}')$ is the normalized spatial distribution of the secondary runaway electrons created. The runaway electron source function is then the sum of n_s and S_x: $S = n_s + S_x$ (note that there is a typo in the expression for S_0 in *Dwyer* [2012], where S_{0p} should be n_{s0}).

[15] Computing the 3-D integral for S_p or S_x at every grid point can be time consuming. We can take advantage of the cylindrical symmetry to perform the integration over the azimuthal direction in advance and save the results in a 3-D matrix to use later. For example, $n_{p0}(\vec{x},\vec{x}')$ is the only term in the integral for S_p that depends on the azimuthal angle. In cylindrical coordinates (r,ϕ,z), $\sqrt{(x-x')^2+(y-y')^2}$ in equation (11) in *Dwyer* [2012] is $(r'^2 + r^2 - 2r'r\cos\phi')$ and so $n_{p0} = n_{p0}(r',\phi',z-z',r)$. The positron source function $S_p(\vec{x},t+\Delta t)$ is then

$$S_p(\vec{x},t+\Delta t) = \mathrm{eff}_p(\vec{x})\exp\left(\frac{\Delta t}{\tau'}\right)\int_0^z\int_0^R vn_{re}(\vec{x}',t)\,\exp\left(-\frac{|z-z'|}{v\tau'}\right) r'\int_0^{2\pi} n_{p0}(r',\phi',z-z',r)\mathrm{d}\phi', \tag{7}$$

where $z = 0$ and $r = R$ define the bottom and outer boundaries of the simulation region, respectively. It is assumed that

the runaway electron avalanche propagates in the positive z direction. Let $G(r', z-z', r) = r' \int_0^{2\pi} n_{p0}(r', \phi', z-z', r)\mathrm{d}\phi'$, which depends only on the numerical grid and needs to be calculated only once. The same technique can also be applied to calculating $S_x(\vec{x}, t+\Delta t)$.

[16] To solve equation (2) numerically, the finite volume method [*LeVeque*, 2002] is used to discretize the system, and the original Scharfetter-Gummel method [*Kulikovsky*, 1995] is applied to calculate the particle flux $\vec{v}n_r - \hat{D}_c^d \nabla n_r$, where $\hat{D}_c^d$ is the diagonal terms of $\hat{D}_c$. The cross-diffusion terms are added separately. For example, the z component of the diffusion flux due to the cross-diffusion term at half grid point is

$$F_{cz}\big|_{ir,iz+1/2} = -D^{zr}\frac{\partial n}{\partial r}\big|_{ir,iz+1/2},$$

where ir and iz are the integer indexes for the grid lines. The derivative $\frac{\partial n}{\partial r}\big|_{ir,iz+1/2}$ is calculated by averaging its values at the locations (ir, iz) and (ir, iz+1), each of which is calculated by using the central difference scheme. The linear equation system resulting from the numerical discretization is solved with successive over-relaxation (SOR) method [*Press et al.*, 1992] and an empirical value of one is found to be a good choice for the relaxation factor allowing fast convergence of the solution.

[17] If the electric field is unvarying in the course of the simulation, for example, because the ionization created by the RFD is negligible, the densities of the runaway electrons and the positrons vary exponentially in time with an e-folding constant τ' but the shapes of the density distributions do not change. The time unvarying shapes of the density distributions can be found by solving the transport equations for the runaway electrons and the positrons for a few iterations in time with the densities obtained from the previous iteration used as the inputs for the current iteration. For each iteration, choosing $\Delta t = \tau_{fb}$, $S_p(\vec{x}, t+\Delta t)$ is first calculated and the positron density is then found by solving equation (2). Knowing the positron density at $t+\Delta t$ allows us to find the runaway electron source function due to the positron feedback at the same moment of time. Together with the runaway electron source function due to the X-ray feedback at this instant, equation (2) can be solved for the runaway electron density at $t+\Delta t$. After each iteration, τ' is updated by $\tau' = \tau_{fb}/\ln(\gamma)$, where γ is calculated by taking the ratio of the total numbers of the runaway electrons at the current and previous iterations. If the electric field changes during the simulation due to either IC lightning leader propagation or polarization of the ionization created by the runaway electrons, the simulation is conducted as follows. The unvarying shapes of the runaway electron and positron density distributions are first found for the initial field distribution as well as the initial τ'. When the field changes by certain fraction, e.g., 10%, the transport equations are solved to update the particle densities and τ'. In addition, since the ionization by the RFDs needs to be followed, it is also necessary to solve the transport equations several times in a time interval of τ' in order to keep the runaway electron and positron densities updated, even though the electric field only changes slightly. In general, the time step Δt for the time-varying field case is not equal to τ_{fb}. To be consistent with the concept of the feedback cycle, the densities and τ' are first found by assuming $\Delta t = \tau_{fb}$ in calculating S_p and S_x. Then the obtained densities are multiplied by $\exp[-(\tau_{fb} - \Delta t)/\tau']$ to get the values at the actual moment of time $t+\Delta t$.

[18] In addition, the diffusion coefficients given by *Dwyer* [2010] describe the diffusion of the particles over a full feedback cycle τ_{fb}. For an arbitrary time step $\Delta t < \tau_{fb}$, the following approximation is used to avoid excessive diffusion for a time step Δt smaller than τ_{fb}:

$$n_{re}^i = \frac{\Delta t}{\tau_{fb}} n_{re}^i + \left(1 - \frac{\Delta t}{\tau_{fb}}\right) n_{re}^{i-1} \frac{\int n_{re}^i \mathrm{d}V}{\int n_{re}^{i-1}\mathrm{d}V},$$

where superscripts i and $i-1$ represent current and previous iterations, respectively.

[19] Another place where the present work is different from that of *Dwyer* [2012] is the calculation of τ_{fb}. For the cylindrical system used in the present work, τ_{fb} is calculated as the runaway electron propagation time, weighted by the positron source function, from the start of the avalanche region to the point $\vec{x}$ assuming they move along the z direction, which is then corrected by an average ratio of the vertical field component to the absolute field strength

$$\tau_{fb} = 2\frac{\int \tau_p(\vec{x}) S_p \,\mathrm{d}V}{\int S_p \,\mathrm{d}V}\left[\frac{\int \frac{|E_z|}{E} S_p \,\mathrm{d}V}{\int S_p \,\mathrm{d}V}\right],$$

where S_p is the positron source function and τ_p is the runaway electron propagation time along the vertical direction. The term in the brackets is a correction for the propagation of the runaway electrons in the radial direction.

2.2. Low-Energy Charged Particle Transport

[20] On average, each runaway electron produces low-energy electron-ion pairs with an ionization coefficient of $8350 \times n\ \mathrm{m}^{-1}$ [*Dwyer and Babich*, 2011]. They then attach to O_2 molecules to form negative ions on a short time scale of a fraction of a microsecond to a few microseconds. Since the space charge resulting from charged particle drift can create an electric field comparable or even greater than the thundercloud field, it is necessary to model the transport of the low-energy charged particles.

[21] The continuity equation for low-energy charged particles (i.e., electrons, positive ions, and negative ions) is solved for this purpose:

$$\frac{\partial n_i}{\partial t} + \nabla \cdot \vec{J}_i = S_i - L_i, \tag{8}$$

where n_i is the number density of the electrons (n_e), the positive ions (n_p), or the negative ions (n_n); $\vec{J}_i$ is the flux density; and S_i and L_i are the source and sink for the ith species; the flux density $\vec{J}_i$ is defined as $(n_i\vec{v}_i - D_i\nabla n_i)$, where $\vec{v}_i = \mu_i\vec{E}$ is the drift velocity, μ_i the mobility of the ith charged species, and D_i the diffusion coefficient. The terms S_i and L_i account for the effects of electron impact ionization, two and three body attachments, and recombination. The ionization and attachment coefficients, the electron mobility, and the electron diffusion coefficient are a function of electric field, which can be found in *Liu and Pasko* [2004] and *Moss et al.* [2006]. The same mobilities and diffusion coefficients of the positive and negative ions as used in *Dwyer* [2012] are adopted in this study. The numerical schemes used to solve equation (8) are described in *Liu and Pasko* [2004], where only the continuity equation for the electrons is solved for simulating the initial propagation stage of conventional

streamers. However, the same numerical techniques have also been applied to solve the ion continuity equations for sprite halos [*Liu*, 2012]. For typical relativistic feedback discharges, the attachment time, which can be as small as a few hundred nanoseconds, is the shortest among all characteristic times of the relevant processes. The simulation time step for solving equation (8) is constrained by this time, which is normally much shorter than the time step for simulating the transport of the runaway particles.

2.3. Intra-Cloud Lightning Leader

[22] The role of the IC lightning in the TGF production by the RFDs is that it can push the system above the feedback threshold ($\gamma > 1$) to quickly increase the numbers of the runaway electrons and the gamma photons produced. The IC lightning is simulated by an expanding volume of enhanced conductivity that becomes polarized in the thundercloud field. This high-conductivity region is modeled as a cylindrically symmetric volume:

$$\sigma = \begin{cases} \sigma_0 \exp(-r^2/2r_0^2) & z_+ < z < z_- \\ \sigma_0 \exp\left(-[(z-z_-)^2 + r^2]/2r_0^2\right) & z \geq z_- \\ \sigma_0 \exp\left(-[(z-z_+)^2 + r^2]/2r_0^2\right) & z \leq z_+ \end{cases}, \quad (9)$$

where r_0 is the radial scale of the discharge (lightning) region, and z_+ and z_- represent the locations of the positive and negative heads of the lightning channel, respectively. In the model,

$$z_- = z_{\text{init}} + r_0;\ z_+ = z_{\text{init}} - r_0;\ \text{with}\ r_0 = r_0^i + 0.5 v_l t,$$

where v_l is the constant lightning propagation speed (bidirectional), r_0^i is the initial radius of the lightning discharge region, and z_{init} is the height of the lightning initiation point. At very low fields, the conductivity is reduced to prevent the electric field from completely vanishing inside the lightning discharge region (see *Dwyer* [2012] for the multiplication factor introduced to reduce the conductivity).

[23] The continuity equation is solved for the space charge density ρ_{IC} from the IC lightning,

$$\frac{\partial \rho_{\text{IC}}}{\partial t} = -\nabla \cdot \vec{J}_{\text{IC}}, \quad (10)$$

where the IC current density $\vec{J}_{\text{IC}} = \sigma \vec{E}$. Finite volume method is again used to discretize the simulation region, and then equation (10) is numerically integrated over time using the Euler method.

[24] Another method used to initiate the relativistic feedback process is to add a region of high-ion density. For this method, the initial positive and negative ion densities follow a similar distribution described by equation (9). The transport of the introduced ions is simulated automatically when solving equation (8).

2.4. Electric Field, Current, Current Moment, Charge Moment Change, and Power

[25] Electric field in the model may have three sources: the thundercloud charge, the space charge from the IC lightning, and the space charge from the RFD process. The thundercloud charge field varies only on long time scales and needs to be calculated once. To find the IC lightning and the RFD space charge fields, Poisson's equation is solved at each time step for the electric potential ϕ:

$$\nabla^2 \phi = -\frac{\rho}{\varepsilon_0}, \quad (11)$$

where ρ is the charge density and ε_0 is the permittivity of free space. The charge density ρ is the sum of the IC space charge density ρ_{IC} and the space charge density from the RFDs, i.e., $e(n_p - n_e - n_n)$. The electric field is then found by $\vec{E} = -\nabla\phi$. Equation (11) is solved numerically with the finite difference method and the SOR method. The numerical technique discussed in *Liu and Pasko* [2006] is employed to obtain accurate solution to electric potential when a small domain containing the discharges is simulated. This technique first calculates the direct integral solution of the electric potential on the boundaries of the simulation domain, and then the potential at interior points is found by using the SOR method with the known boundary potentials.

[26] Current I_z, current moment M, charge moment change (or dipole moment charge) CMC, and power P are calculated as follows:

$$I_z = \int |J_z|\, \mathrm{d}a,\ M = \int |J_z|\, \mathrm{d}V,\ \text{CMC} = \int M\, \mathrm{d}t,\ P = \int \vec{E} \cdot \vec{J}\, \mathrm{d}V, \quad (12)$$

where $\vec{J}$ is the volume current density, J_z is its vertical component, and P is the work done on the charge by the electric field. Note that M is the time rate of change of electric dipole moment, which leads to the integral equation for the charge moment charge CMC. The current moment M is a measure of the inductive component of the electric field produced by the discharge, and its derivative is a measure of the radiation field component. For plotting purpose, the absolute value of J_z is used to calculate I_z and M, because J_z of +IC flashes and relativistic feedback discharges is negative as thundercloud electric field points in the negative z direction.

3. Results

3.1. Single-Pulse TGFs

[27] We first present the simulation results of a relativistic feedback discharge triggered by an IC lightning leader developing between the negative and positive charge layers inside a thundercloud. The same parameters as in *Dwyer* [2012] are used here for modeling the thundercloud charges and the IC lightning. The thundercloud negative and positive charge regions are modeled using Gaussian charge distributions located at 10 and 15 km, respectively. The Gaussian sigma of the upper positive charge distribution is 800 m in the z direction and 3000 m in the horizontal directions. The Gaussian sigma of the negative charge distribution is 800 m in the z direction and 1000 m in the horizontal directions. The total charges are $\pm$36.5 C in the two regions, respectively. The electric dipole moment of this system is 182.5 C km, which can be found as follows. Since the net charge of the system is zero, the dipole moment is independent of the choice of the origin of the coordinate system. If we choose the center of the negative charge region as the origin, the contribution from the negative charge to the dipole moment vanishes. The contribution from the positive charge is $\int \rho(5\,\text{km}\,\hat{z} + \vec{R})\, \mathrm{d}V = \int \rho(5\,\text{km}\,\hat{z})\, \mathrm{d}V + \int \rho \vec{R}\, \mathrm{d}V$, where $\vec{R}$ is the separation vector from the center of the positive charge

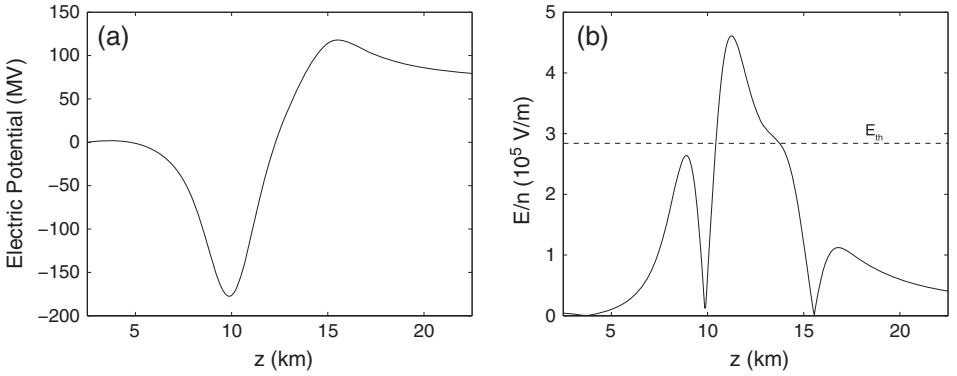

Figure 1. The axial profile of the (a) electric potential and (b) electric field strength of the thundercloud charges.

region to the point of interest. The last integral vanishes again, and the second to last integral gives 36.5 C × 5 km = 182.5 C km for the strength of the dipole moment.

[28] Figure 1 shows the axial profile of the electric potential and electric field strength of the thundercloud charge. The reference point for the electric potential is set on the symmetry axis at z = 2.5 km, which is the lower simulation boundary for solving Poisson's equation. The upper boundary is at 22.5 km. The maximum potential difference between the upper positive charge region and lower negative charge region is about 300 MV. Such a potential difference inside a thundercloud is not unreasonable according to balloon measurements [*Stolzenburg and Marshall*, 2008]. The electric field exceeds the threshold field of RREAs from 10.4 to 13.7 km, and E/n is peaked at 11.3 km with a value of 4.6×10^5 V/m. It should be noted that a smaller simulation domain, z spanning from 10 to 15 km, is used for solving the transport equations of particles. In the simulation results presented below, densities of various particles are available only in this region.

[29] The simulation is initiated by introducing an IC lightning discharge at t = 0 ms. The parameters for the IC lightning are z_{init} = 11.3 km, $v_l = 5 \times 10^5$ m/s, r_0^i = 100 m, and $\sigma_0 = 7.2 \times 10^{-6}$ S/m. As the lightning develops according to equation (10), its high conductivity volume becomes polarized, and negative charge appears around its upper end while positive charge around its lower end. Consequently, the thundercloud field is screened out of this volume and the fields in the regions around the two ends are strongly enhanced. Relativistic runaway electron avalanches develop from the upper end of the IC lightning toward the positive thundercloud charge region. As the IC lightning continues to propagate and expand, the relativistic feedback discharge becomes stronger. The feedback factor γ can temporarily exceed 1, and the RFD produces large numbers of runaway particles, energetic photons, and low-energy charged particles.

[30] The current moment, the feedback factor, and the gamma photon emission rate are shown in Figure 2. The discharge becomes self-sustaining (γ = 1) at $t \simeq 0.36$ ms and a TGF pulse begins to form at this time and reaches its peak at $t \simeq 0.65$ ms that corresponds to the time the feedback factor returns to be smaller than 1. The falling of γ or the quenching of the RFD process is caused by partial discharging of the avalanche region by the ionization created by the RFD process, which is discussed in detail later in this section.

[31] The current moment shown in the figure includes the contributions from both of the IC lightning and the RFD process. As discussed in sections 2.3 and 2.4, space charge densities from the IC lightning and the RFD process are separately calculated, which allow us to differentiate the IC lightning current from the current associated with the RFD process. The IC lightning current results from the conductivity specified in its volume (i.e., the motion of charged particles is not explicitly simulated), while the RFD current is carried by the motion of the electrons and ions created. The propagating and expanding IC lightning causes a steady increase in the current moment. The narrow pulse between 0.6 and 0.7 ms superimposed on the IC lightning component is produced by the RFD process. This pulse overlaps with the falling stage of γ and is centered around $t \simeq 0.65$ ms when γ decreases to 1. Note that although γ decreases between 0.6 and 0.65 ms, it is still greater than 1 so that the numbers of particles still increase rapidly in this period. The RFD current moment pulse approximately coincides with the TGF pulse, after considering that one is plotted on a linear scale and the other on a logarithmic scale.

[32] The RFD current moment pulse has a peak value of 24 kA km and a full width at half maximum (FWHM) width of 40 μs. After the pulse, the current moment due to the motion of the ions created by the RFD slowly varies between 1.6 and 1.8 kA km. The charge moment change due to this current is about 1 C km just after the pulse and steadily increases to 1.6 C km by the end of the simulation. As a comparison, the charge moment change caused by the IC lightning reaches 22.3 C km at the end of the simulation that seems to be consistent with the 90 C km charge moment change, in several milliseconds, of the IC lightning associated with the TGF event analyzed by *Lu et al.* [2010]. The space charge created by the IC lightning is distributed around the conducting volume of the IC lightning (the dark blue region in Figure 3a with the negative charge around the upper tip and positive charge around the lower tip). The peak power of the work done by the electric force on the charged particles created by the RFD process is about 1.2×10^{12} W. The results from *Dwyer* [2012] are plotted in dashed lines in Figure 2. As can be seen, the present work is in an excellent agreement with that of *Dwyer* [2012] and only small differences exist in the occurrence time, magnitude, and width of the pulse.

[33] Figure 3 shows the distributions of the reduced electric field E/n, the runaway electron density, the run-

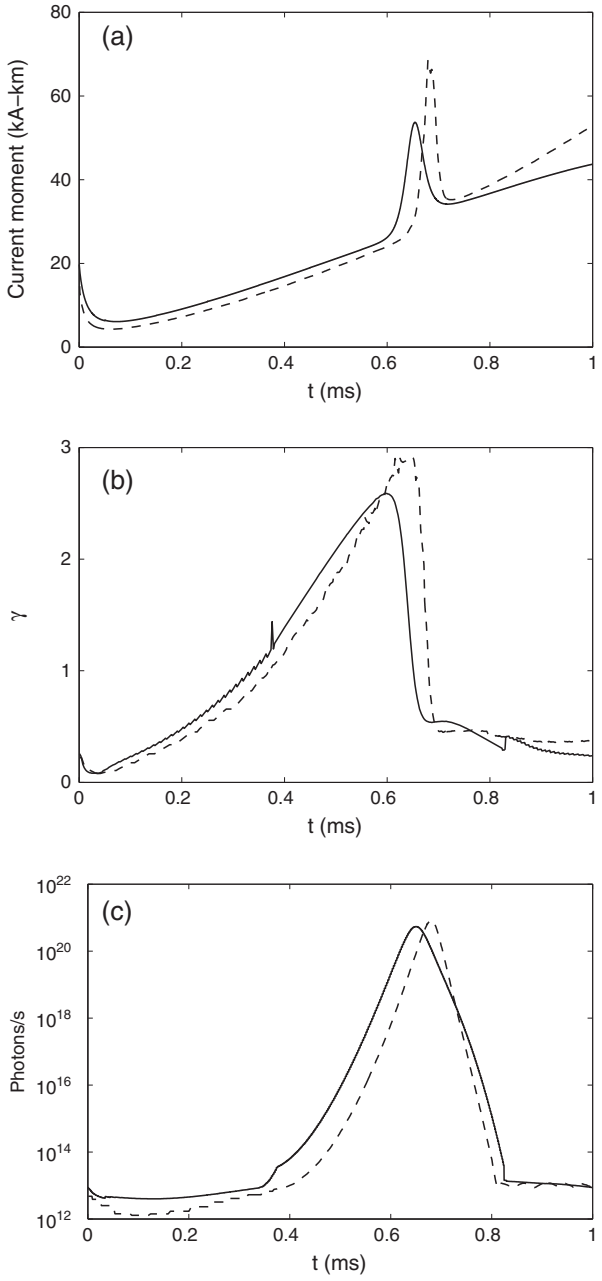

Figure 2. The parameters of a relativistic feedback discharge producing a single-pulse TGF: (a) current moment, (b) feedback factor, and (c) gamma ray flux at 15 km altitude versus time (see *Dwyer* [2012] on how the intensity of the gamma rays is calculated at 15 km altitude, regardless of the gamma source location). Solid lines are the results from the present work and dashed lines are from *Dwyer* [2012].

away positron density, and the positron source function at t = 0.65 ms, the moment of the TGF pulse peak. The runaway electrons and positrons are concentrated at different locations in the avalanche region, because the RFD model equation describes the steady state density distributions of the runaway particles given their sources at a particular moment of time. The seed runaway electrons are produced by the positrons at the beginning of the avalanche region, i.e., the upper end of the IC lightning, which then produce more runaway electrons via RREAs as they travel toward the end of the avalanche region (near the top boundary of the plot), where the runaway electron density is maximized. The distribution of the positron source function roughly follows the runaway electron density distribution, and it is maximized in the same region. The positrons are produced there and propagate along the field line back to the beginning of the avalanche region. The positron annihilation length in the avalanche region is several kilometers long and nearly all the positrons converge to the tip of the lightning. The positron density then decreases rapidly in the IC lightning volume as their annihilation length becomes very short in the low-field IC volume.

[34] To understand how the RFD is quenched by the ionization produced by itself, we can inspect the axial profiles of the electric field and potential. The solid and dashed lines in Figure 4a show the electric field with and without the RFD, respectively. Although the RFD becomes self-sustaining at t = 0.36 ms, not enough numbers of electrons and ions are produced to modify the thundercloud and lightning field before 0.6 ms. Consequently, the solid lines completely overlap with the dashed lines before 0.6 ms. The density distributions of the electrons and ions created by the runaway electrons generally follow that of the runaway electrons (the profiles of the electrons and ions are shown in Figure 5). As shown in Figures 3a and 3b, the runaway electron density is maximized in the volume above the high-field region around the IC lightning. The electrons and ions are also concentrated in that region, forming an enhanced conductivity volume around 14 km altitude. After 0.6 ms, the electric field in this volume is quickly reduced, while the field around its lower and upper ends is enhanced. This can be seen by comparing the solid lines to the dashed lines at 0.8 and 1 ms in Figure 4a.

[35] Figure 4b shows the electric potential profiles spanning from 2.5 to 22.5 km at the time before, during, and after the RFD. The gradient of the potential is reduced inside the IC lightning while increased just outside it. The IC lightning has reached the lower negative thundercloud charge region and has partially neutralized the charge there, increasing the potential around 10 km altitude. Since the upper tip of the IC lightning is still far away from the thundercloud positive charge layer, only a slight decrease in potential is found there. On each curve except the one for the ambient potential at t = 0 ms, the left black dot marks the beginning of the avalanche region and the right dot marks its end. Compared to its values at 0.4 and 0.6 ms, the potential after the RFD discharge (e.g., t = 0.8 ms) is reduced only slightly in the region between the IC lightning and the upper thundercloud charge. However, the reduction in the electric field around 14 km altitude shown in Figure 4a compresses the avalanche region toward the IC lightning tip and significantly reduces the potential difference between the two bounding points of the avalanche region. This is the reason why the RFD is quenched. Figure 4c shows that the potential difference across the avalanche region is reduced from 150 MV before the RFD to 100 MV after the discharge. In summary, a conducting volume is produced near the end of the avalanche region by the RFD. The space charge appearing from the polarization of the volume lowers the field inside below the RREA threshold field and squeezes the avalanche region. This leads to a significant loss in the potential difference

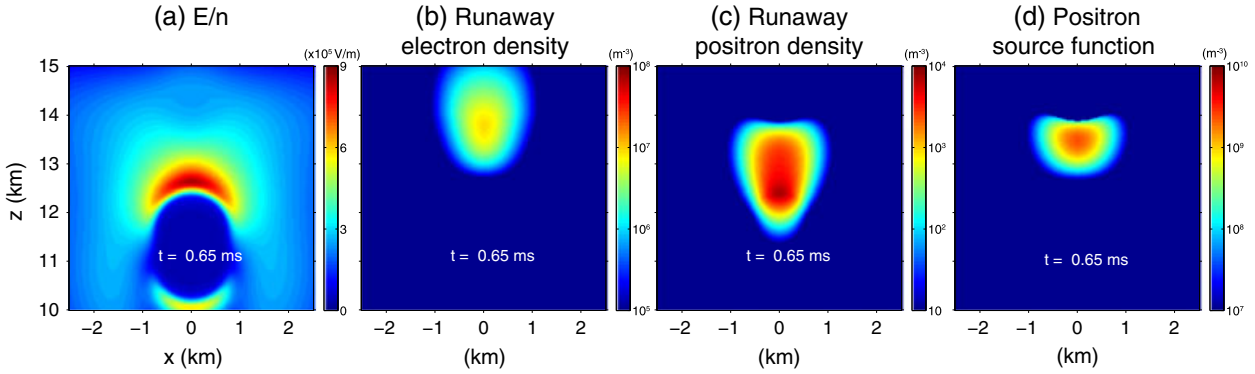

Figure 3. The cross-sectional views of the following quantities at 0.65 ms, the moment of the relativistic feedback discharge producing the gamma emission peak. (a) Reduced electric field, (b) runaway electron density, (c) runaway positron density, and (d) positron source function.

across the avalanche region and quenches the discharge. However, the potential profile is not significantly modified. A simple example to illustrate this is a discharge developing between two electrodes maintained at different potentials. Suppose that the discharge originates from the anode and propagates to the cathode. The potential difference between its tip and the cathode is of course deceasing while the discharge with an imperfectly conducting channel extends. In our case, the decrease is made worse by an increase in the potential of the cathode and a decrease in the potential of the anode.

[36] Note that the large initial potential difference (more than 200 MV) shown in Figure 4c is obtained for the avalanche region extending from 10.4 to 13.7 km. The electric field becomes smaller than E_{th} around the initiation point of the IC lightning a few microseconds later, splitting the avalanche region into two parts. After the splitting, the potential difference shown in the figure corresponds to the avalanche region from the upper IC lightning tip to the upper positive charge layer. Although the potential difference stays around 150 MV before 0.6 ms, the feedback factor γ increases (see Figure 2b) because the IC lightning is expanding. The ionization level around 14 km altitude increases steadily (see Figure 5), and it reaches a level high enough around 0.6 ms to relax the field there and quench the discharge.

[37] As mentioned above, the density distribution of the low-energy electrons created by the relativistic feedback discharge is similar to the runaway electron density distribution, because once created by the runaway electrons, they are converted to negative ions in a fraction of a microsecond to a few microseconds. The positive and negative ions last much longer (more than tens of milliseconds). The axial profiles of the electrons, positive ions, and negative ions at several moments of time are shown in Figure 5. The electrons are created in the runaway electron avalanche region, and their density quickly increases when the feedback factor of the RFD becomes greater than 1. After the RFD is quenched around 0.7 ms, they are lost rapidly due to the attachment process. The positive ion density also quickly increases when $\gamma > 1$, but their density is unvarying after 0.7 ms (not shown in the figure) because the recombination with the negative ions becomes effective only after several milliseconds. The negative ion density profiles (not shown in the figure) are similar to the positive ions'. The total number of the positive or negative ions created by the RFD pulse is about 0.5–1 $\times 10^{23}$. The profiles of the charge density created by the RFD process show that a positive charge region

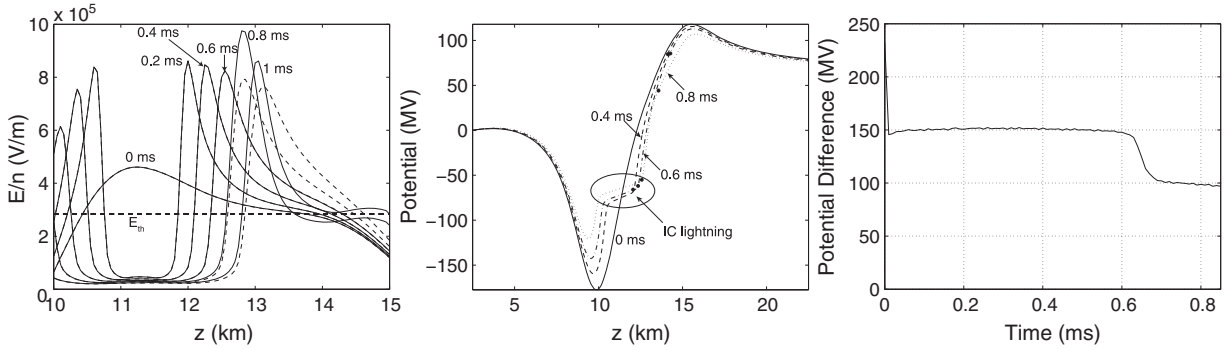

Figure 4. (a) The axial profiles of the reduced electric field at several moments of time. The solid lines show the electric field with the RFD. The dashed lines show the field without the RFD, and they overlap with the solid lines at 0.2, 0.4, and 0.6 ms, i.e., before the RFD produces enough ionization to modify the field. (b) The axial profiles of electric potential before, during, and after the RFD. (c) The time variation of the potential difference across the RREA region between the upper tip of the IC lightning and the positive thundercloud charge layer.

is formed around 13 km and a negative charge region at 14.5 km. The total amount of charge in these two regions is about ±0.5 C right after the pulse and about ±1 C at 1 ms. After 0.8 ms, most of electrons are converted to negative ions, and the negative charge around 14.5 km is caused by an excess of negative ions.

[38] With an ion mobility of (1.4–1.9 $\times 10^{-4}$ m^2/V/s)/n [*Dwyer*, 2012], the Maxwellian relaxation time corresponding to the peak ion density of about 10^{14} m^{-3} at that altitude (13.5 km) is a half millisecond, which is much longer than the width of the pulse. Given that the electric field is 5.4 × 10^4 V/m at 13.5 km at 0.65 ms, the field-dependent electron mobility is approximately 0.46 m^2/V/s (see *Moss et al.* [2006] for the field dependence of the electron mobility; however, it should be noted that an exponentially decreasing atmospheric density with a scale height of 7.2 km is used here in order to be consistent with the work of *Dwyer* [2012]). With the electron density reaching about 10^{13} m^{-3} at 13.5 km altitude (see Figure 5a), the corresponding electronic conductivity is about 7.4 × 10^{-7} S/m and the Maxwellian relaxation time is about 10 μs. Therefore, the space charge shown in Figure 5c that quenches the RFD and makes the TGF pulse short, is mainly caused by electron drift.

3.2. Multiple-Pulsed TGFs

[39] As shown by *Dwyer* [2012], a self-propagating discharge, named as a relativistic feedback streamer, can result from the relativistic feedback process, if a large potential difference exists in the high-field region in thunderclouds. Once the relativistic feedback streamer is formed, it can propagate into a region with an electric field below the runaway electron avalanche threshold field. It was also found that the relativistic feedback streamer propagates in a pulsed fashion and can generate multiple-pulsed TGFs observed by BATSE. The pulsing comes about from the two time scales associated with the low-energy electron and the ion discharge times. As discussed in the previous section, the RFD is quenched when a large number of electrons and ions are produced in the avalanche region. The electrons quickly attach to air molecules to form negative ions, and a conducting channel consisting of positive and negative ions is produced in this way, i.e., the region above 13.5 km in Figure 5. If the IC lightning stops propagating after the RFD is quenched, ion drift in the RFD channel will gradually remove the negative charge in Figure 5c and pump more positive charge in the tip of the channel. This will lower the field in the channel and raise the tip potential to restore the potential difference across the avalanche region. As a result, the RFD can become self-sustaining again and add a new segment to the current channel tip. In this way, a self-propagating relativistic feedback streamer is formed. The role played by the IC lightning is to enhance the thundercloud field to create favorable conditions for the relativistic feedback discharge, and the IC lightning becomes unnecessary if the self-propagating relativistic discharge with a conducting channel can produce its own avalanche region.

[40] In the present work, the pulsed propagation of the relativistic feedback streamer and associated multiple-pulsed TGFs are also seen from the simulations. In addition, the simulations also show that the propagation of the streamer may become continuous after going through an initial pulsed

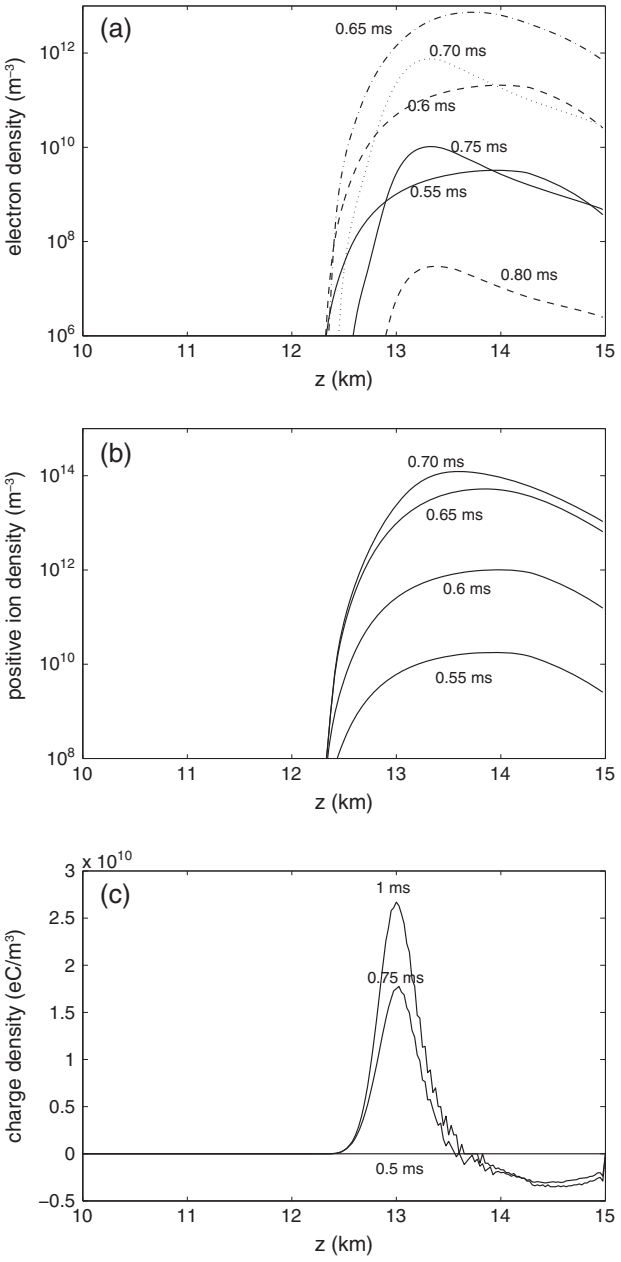

Figure 5. The axial profiles of the relativistic feedback discharge at different moments of time. (a) Electron density, (b) positive ion density, and (c) charge density.

stage. An example of such relativistic streamers and associated TGF pulses is shown in Figures 6–9. The simulation was initiated by injecting a column of enhanced ion density with a radius of 250 m that extends from 16 km down to 14 km altitude. The initial peak ion density is 9.4 × 10^{14} m^{-3} for both the positive and negative ions. A uniform ambient electric field was set to 2.6 × 10^5 V/m × n, which is slightly smaller than the runaway electron avalanche threshold. The ion column might represent a lightning discharge or it might represent the ions produced by the runaway feedback discharge.

[41] As shown in Figure 6, the properties of the relativistic feedback streamer are similar to a conventional

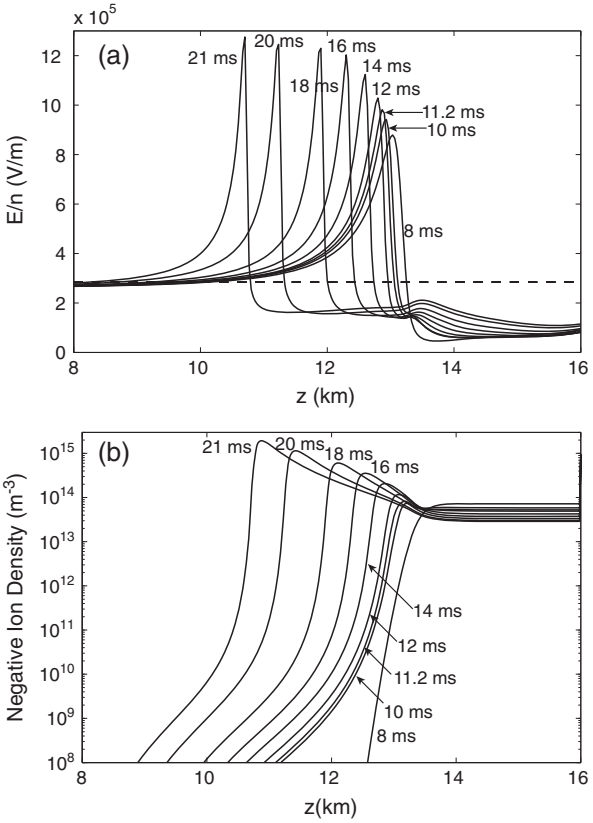

Figure 6. The axial profiles of (a) electric field and (b) negative ion density of a relativistic feedback streamer propagating in a uniform electric field of 2.6×10^5 V/m $\times n$, which is slightly below the runaway electron avalanche threshold field.

positive streamer. The electric field is highly enhanced in the streamer head, and the channel field is smaller than the ambient field. The feedback process works like the photoionization process by creating seed runaway electrons ahead of the head to initiate RREAs propagating toward the streamer head. However, the head field of the relativistic streamer tends to increase after the streamer is formed, while the head field of a positive streamer stays constant if the propagated distance is not too long. In addition, the ion density of the relativistic feedback streamer head increases as it propagates forward in contrast to the constant electron or ion density in the positive streamer head.

[42] Figure 7 shows that several TGF pulses are generated by the relativistic feedback streamer initially. The time separation between successive pulses decreases and the pulse height varies a little. Each pulse is approximately symmetric (with the falling time being slightly longer than the rise time), and the FWHM width of individual pulses increases slightly from 200 to 400 μs.

[43] After the first two pulses, the oscillating magnitude of γ around 1 decreases and eventually settles to $\gamma \simeq 1$ (slightly larger than 1). The photon flux pulses start to overlap each other until they completely blend together, forming a long TGF pulse with steadily increasing fluxes. At this stage, the relativistic feedback streamer propagates continuously in the ambient field. This occurs when the Maxwellian relaxation time of the channel immediately behind the head is comparable to the Maxwellian relaxation time in the avalanche region (see the next section for detailed discussion).

[44] The cross-sectional distributions of the negative ion density at several moments of time are shown in Figure 8. From Figures 6 and 8, it can be seen that the relativistic feedback streamer accelerates, which is similar to the conventional positive streamer. However, the acceleration of the conventional positive streamer is typically accompanied by the expansion of the streamer head, and its head radius is linearly proportional to its length, keeping the streamer head field from increasing [*Liu and Pasko*, 2004]. However, the head size of the the relativistic feedback streamer does not increase linearly with its length. As the streamer extends, the potential difference between the streamer head and the ambient Laplacian potential builds up because the field in the newly added channel segment is smaller than the ambient field (this is partially compensated by the increase in the electric field in the old channel as shown in Figure 6a). Together with a decreasing radius of the streamer head, it leads to an increasing field in the relativistic feedback streamer head.

[45] Figure 9 shows the cross-sectional views of the field, the runaway electron density, the runaway positron density, and the positron source function at the time of the second TGF pulse (t = 11.2 ms) and at the time of the relativistic feedback streamer propagating continuously (t = 21 ms).

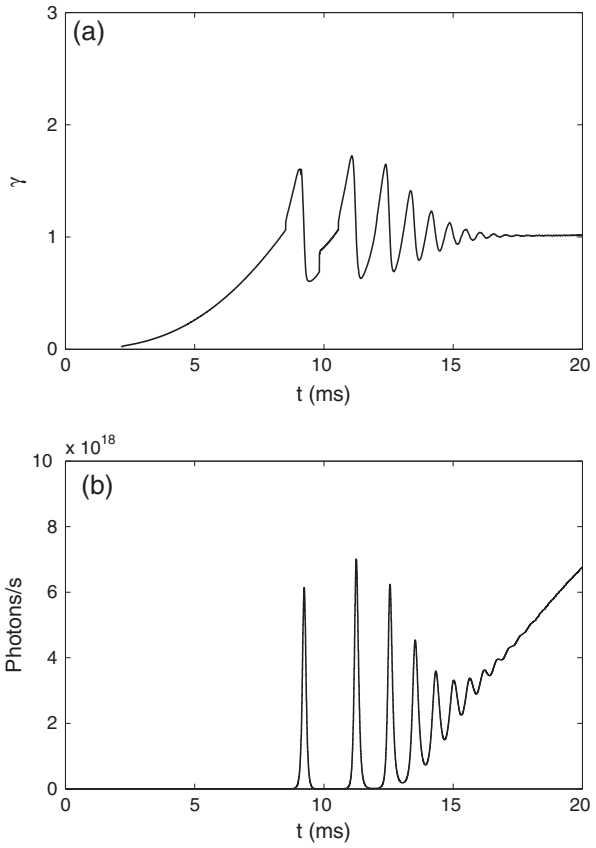

Figure 7. (a) The feedback factor of the relativistic feedback discharge producing the feedback streamer shown in Figure 6. (b) The gamma ray flux of the feedback streamer at 15 km altitude versus time.

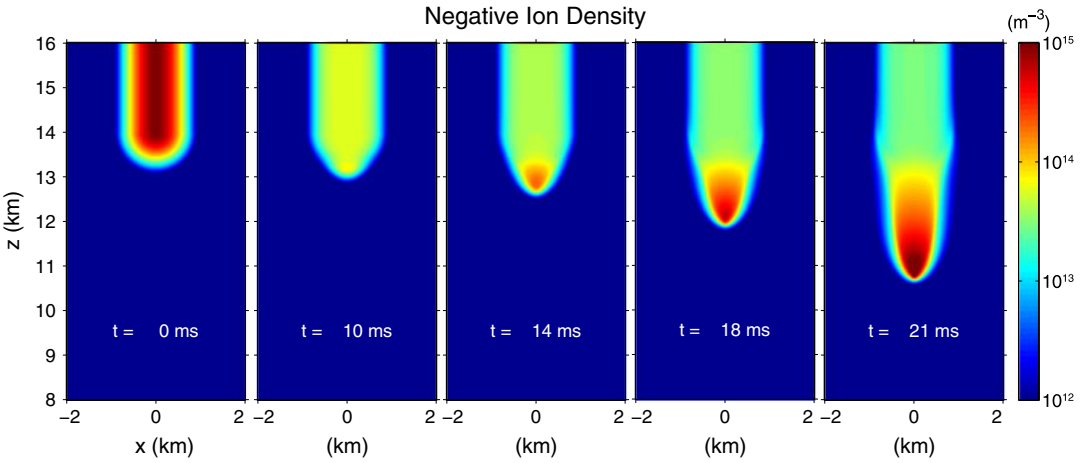

Figure 8. The cross-sectional views of the negative ion density of the relativistic feedback streamer at several moments of time.

The electric field is strongly enhanced in the head because of the conducting streamer channel. The runaway electrons are produced in the high field region and run away in the opposite direction of the electric field (approximately upward). Their density decreases as they enter the low-field region in the channel because the avalanche length turns into negative in that region. The maximum positron density is several orders of magnitude smaller than that of the runaway electron density, and the volume of high positron density is much more extended than that of the runaway electron density. This can be understood as follows. The distribution of the positron source function shows that the positrons

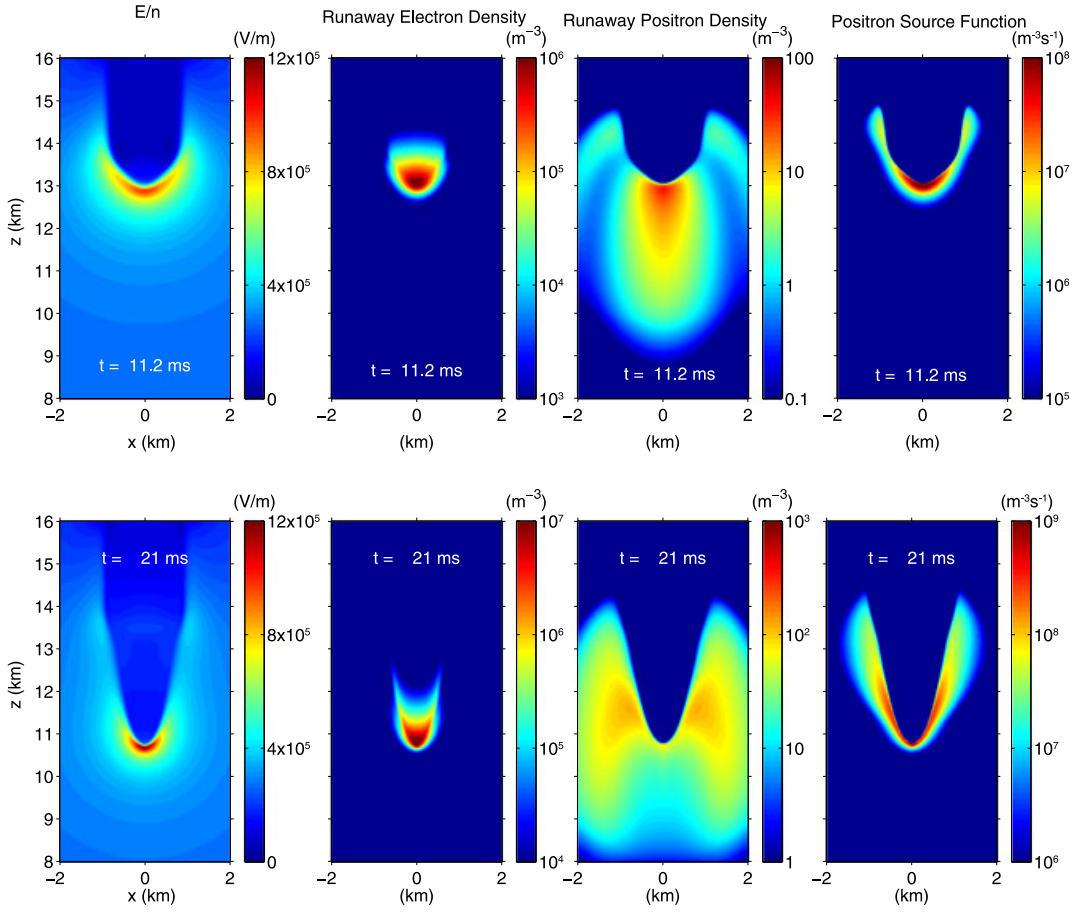

Figure 9. The cross-sectional views of the reduced electric field, runaway electron density, runaway positron density, and positron source function during pulsing (t = 11.2 ms) and continuous (t = 21 ms) propagation of the feedback streamer.

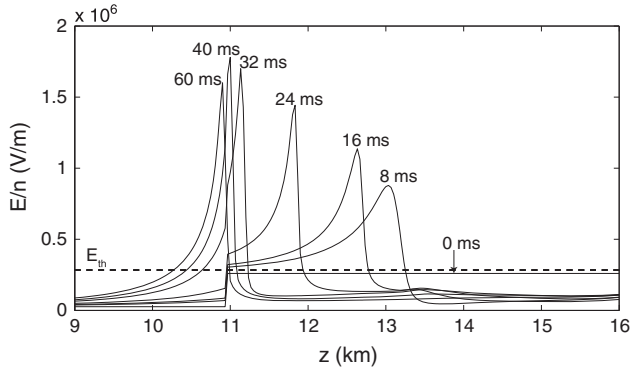

Figure 10. The axial profiles of the electric field of a relativistic feedback streamer propagating in a nonuniform thundercloud field. The ambient field below 11 km altitude is a factor of 10 smaller than its value, 2.6 $\times 10^5$ V/m $\times n$, above.

are effectively produced by the runaway electrons around the tip of the streamer only, because of three factors: (1) the runaway electrons are concentrated in the tip; (2) the positrons are produced only when the local field is greater than the runaway electron avalanche threshold field; and 3) the produced positrons are distributed as a cone. Because the runaway model equation describes the steady state densities of the runaway particles given their sources at a particular moment of time, the positrons are produced around the tip and move away from the streamer tip along the field lines while experiencing diffusion and annihilation. Since the electric field in the region around the tip is larger than the streamer channel field, the positron annihilation length in that region is much longer than the *e*-folding length for runaway electron loss in the low-field region of the streamer channel. The positrons can move along the field lines for a much longer distance, forming an extended volume of high positron density.

[46] As the head field of the relativistic streamer continues increasing, more and more runaway electrons are produced as well as electrons and ions. The propagation of the relativistic streamer approaches an instability several milliseconds after 20 ms. A plausible physical mechanism for stopping the relativistic feedback streamer from producing excessive numbers of high-energy particles is that the streamer runs out of the high-field region for propagation. Figure 10 shows the axial profiles of the electric field of a relativistic streamer propagating in a nonuniform thundercloud electric field. The ambient field above 11 km is the same as before, 2.6 $\times 10^5$ V/m $\times n$, and is 10 times smaller below. Although the streamer head seems to successfully cross the field transition altitude at 11 km around 40 ms, the field below that altitude is too small to support the propagation of the streamer, which dies gradually. An interesting investigation for future research would be to find the minimum field required for the propagation of the relativistic feedback streamer.

[47] A complex sequence of TGF pulses is produced by this streamer, which is shown in Figure 11. The feedback factor oscillates around 1 initially with decreasing magnitude, and the oscillating magnitude becomes very small around 20 ms, which is similar to the previous case shown in Figure 7 except that γ settles to 1 smoother in that figure. However, starting around 23 ms, the oscillating magnitude increases rapidly and several spikes appear on the curve. Finally, the magnitude decreases again after reaching its peak around 28 ms, signaling that the streamer is dying. The initial TGF pulses have a FWHM width of 170–180 μs, between 18 and 24 ms appears to be formed, a long TGF pulse superimposed by small and short pulses, and the subsequent narrow pulses have a width of 40 μs. The time scales of this sequence of TGF pulses encompass all durations of observed TGFs from space by BATSE, RHESSI, and Fermi.

[48] The negative ion density distributions at several time instants, corresponding to the TGF pulses of different durations, are shown in Figure 12. Once the relativistic feedback streamer is formed, it accelerates with a sharpening head and increasing head ion density before 28 ms. After that time, the head hardly moves forward and the density in the head is also decreasing. From Figures 10–12, it can be seen that the duration of a single TGF pulse seems to be related to the peak field and the size of the high-field region in the streamer head. The long TGF pulse is formed when the ion density in the streamer head is high enough so that there is no temporary reduction in the streamer tip potential during its propagation.

[49] The relativistic feedback streamer can produce a charge moment change comparable to that by large IC lightning. The first streamer leads to a charge moment change of 33 C km from the moment when γ becomes greater than 1 for the first time to the end of the simulation at 21 ms. The second streamer results in 40 C km by the end of the simulation at 60 ms. It seems that the relativistic feedback

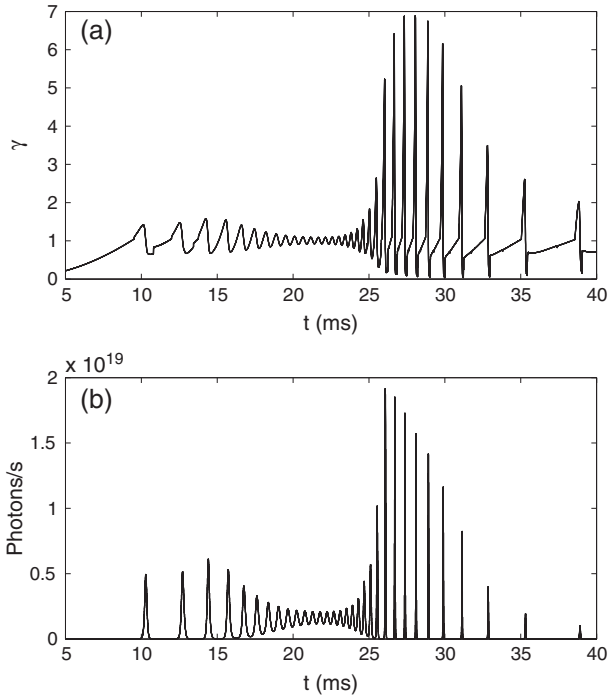

Figure 11. The (a) feedback factor and the (b) gamma photon production rate associated with the relativistic feedback streamer developing in the nonuniform electric field shown in Figure 10.

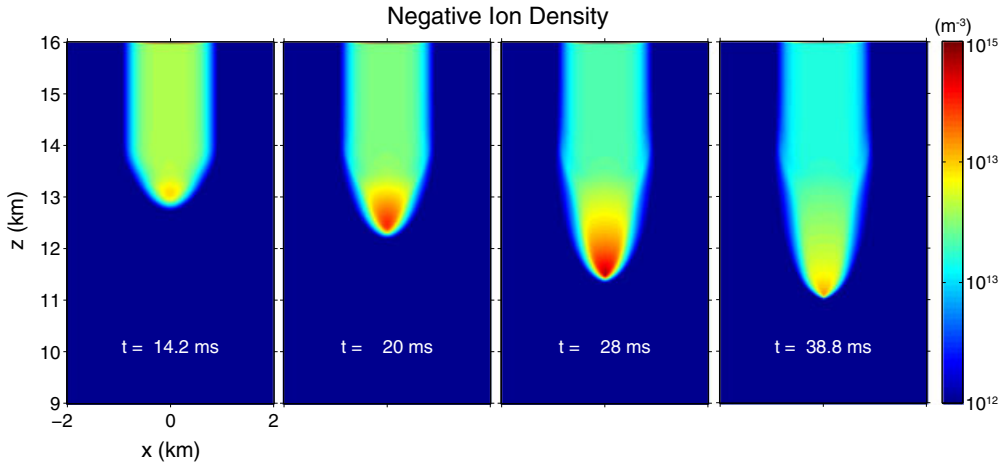

Figure 12. The cross-sectional views of the negative ion density at several moments of time of the feedback streamer in the nonuniform electric field.

streamer could be an important component in thundercloud charge dynamics.

[50] Finally, we compare our simulation results with observations. Figure 13 shows five multi-pulsed TGFs measured by CGRO/BATSE: 3925, 2185, 3813, 6185, and 8006. The vertical axis limits for all panels are set the same except the third panel, where a bigger upper limit is necessary to fully show the first peak of that TGF. The time windows of all panels are 40 ms, the same as that of Figure 11. The TGF events are assembled in time in order to emphasize the resemblance between the simulation results and the measurements. The first and second panels show well-separated pulses that are similar to the initial pulses in Figure 11b in terms of the pulse width and separation, and the trend of increasing pulse magnitude. Note there may be some features immediately following the last peak of each event. The pulses of the TGF shown in the third panel exhibit decreasing pulse magnitude, and the pulses after the first one appear to ride on a wide, smoothly varying pulse. The fourth panel shows a wide TGF pulse, possibly superimposed by smaller pulses. The third and fourth panels together look very similar to the photon production rate curve between 15 and 25 ms in Figure 11b. The last TGF with varying pulse magnitudes appears to be similar to the simulation curve between 25 and 40 ms. It is amazing that the development of a relativistic feedback streamer in a relatively simple field configuration can reproduce so many features of the ensemble of the observed multi-pulsed TGFs. The fact that only a subset of the pulse profile is observed might be explained by lightning starting the system in a state similar to that produced partway through the simulation. Lightning or corona discharges from hydrometeors could also be initiated in the high-field region produced by the relativistic feedback streamer (see section 4.2), terminating the event prematurely.

4. Discussion

4.1. TGF Pulse Width and Continuous Propagation of Streamer

[51] In this section, we explain several interesting features of the simulation results presented in the preceding section. For the isolated pulse produced by the relativistic feedback streamer, the pulse of the feedback factor γ is generally wider than the photon pulse. This is because the TGF pulse approximately corresponds to the falling stage of the feedback factor pulse (see Figures 7 and 11). Although γ is decreasing in this stage, the photon production rate still increases when $\gamma > 1$ and it decreases only when γ becomes smaller than 1. Because of the exponential variation nature of the relativistic feedback discharge, a sharp TGF pulse is formed and centered around the moment of $\gamma = 1$.

[52] As mentioned earlier, the decrease of γ is caused by partial discharging of the electric field in the avalanche region by the ionization created by the relativistic feedback discharge. For each pulse, the electron Maxwellian relaxation time is shortest at the moment of γ falling below 1, while τ' takes its minimum value $\tau'_{\min}$ at the peak of the γ pulse. During the falling stage of the γ pulse, the Maxwellian relaxation time is on the order of $\tau'_{\min}$. For wide pulses, the Maxwellian time is normally greater than $\tau'_{\min}$, but for narrow pulses, the Maxwellian time at $\gamma = 1$ could be smaller than $\tau'_{\min}$. In general, if $\tau'_{\min}$ is small, then the Maxwellian relaxation time is also small. When the electric field decreases with a time scale on the order of $\tau'_{\min}$, the photon production rate by the RFD process should also vary on the same time scale. The TGF pulse width is therefore on the order of $\tau'_{\min}$. This suggests that the smaller this $\tau'_{\min}$ is, the narrower the TGF pulse. The very narrow TGF pulses in Figure 11 are consistent with very small $\tau'_{\min}$ at the peak of the γ pulse, which is $\sim$10 μs and about a factor of 5 smaller than that of typical wide pulses. The small $\tau'_{\min}$ is caused by a combination of small τ_{fb} and large γ for those pulses. The small τ_{fb} is implied by the very narrow field pulse shown in Figure 10. Therefore, the measured widths of TGF pulses, corrected for Compton-scattering delay and instrumental deadtime effects, by BATSE, RHESSI, and Fermi represent the shortest *e*-folding time of the RFD.

[53] As shown in section 3.2, the unusually long (several milliseconds) TGF pulses observed by BATSE can be produced by the relativistic feedback streamer when it propagates continuously. Given that the peak ion density in the channel immediately following the streamer head reaches about 3–10 $\times 10^{14}$ m^{-3} at this stage (see Figures 6 and 12),

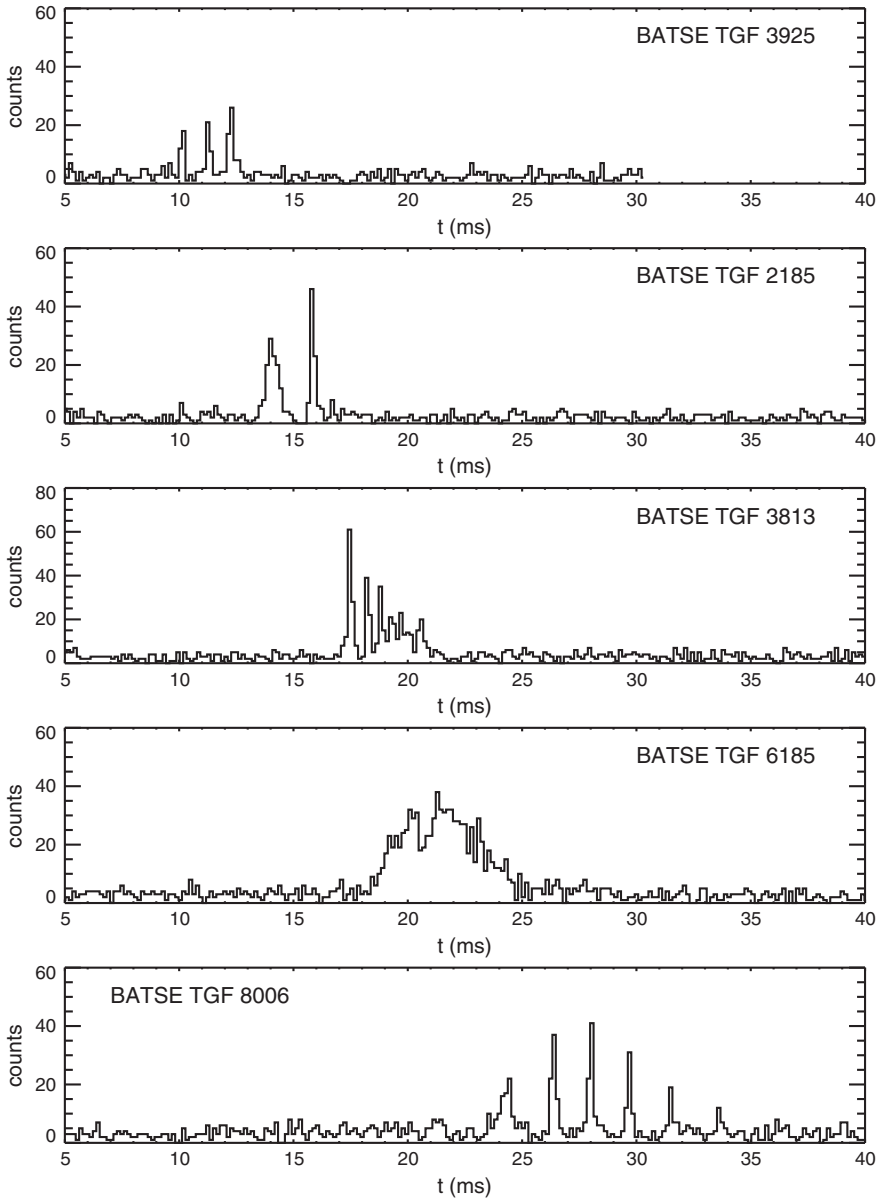

Figure 13. Gamma ray counts rates versus time as measured by CGRO/BATSE for five multi-pulsed TGFs (triggers 3925, 2185, 3813, 6185, and 8006). Data courtesy of Jerry Fishman (http://gammaray.msfc.nasa.gov/batse/tgf/. These plots can also be derived from archived spacecraft data at http://heasarc.gsfc.nasa.gov).

the corresponding Maxwellian relaxation time scale at 11 km altitude is 40–120 μs. The electron density in the streamer head during this stage is 3–10 $\times 10^{12}$ m^{-3}, resulting in a Maxwellian relaxation time of 22–75 μs. This suggests that the relativistic feedback streamer enters the continuous propagation mode when the streamer channel ion Maxwellian relaxation time is comparable to the Maxwellian relaxation time in the streamer head due to electronic conductivity. Under this condition, the temporary reduction in the streamer tip potential is minimized and the streamer propagates continuously.

4.2. Possible Initiation of Conventional Streamers and Leaders from the Relativistic Feedback Streamer Heads

[54] In this section, we discuss the possibility of initiation of conventional streamers and leaders from the relativistic feedback streamer heads in view of recent modeling results on streamers [*Liu*, 2010; *Liu et al.*, 2012; *Sadighi et al.*, 2011; *Kosar et al.*, 2012] and streamer-to-leader transitions [*Riousset et al.*, 2010; *da Silva and Pasko*, 2012]. The conventional streamer and leader are the precursors of lightning initiation, and their initiation has been an important subject for lightning initiation research. To initiate the conventional streamers, the applied electric field must exceed the conventional breakdown threshold field E_k, which is defined by the equality of the ionization and dissociative attachment coefficients [*Raizer*, 1991, p. 135] and is about 3.2×10^6 V/m $\times$ n in air. Several recent studies investigated the electron detachment process from O^- ions, which are the product of the electron two-body attachment process, and found that it is possible that the ionization degree of air increases in an electric field smaller than E_k, particularly

in the middle and upper atmosphere where the three-body attachment process is negligible [*Gordillo-Vázquez*, 2008; *Liu and Sentman*, 2010; *Luque and Gordillo-Vázquez*, 2011; *Liu*, 2012]. If a subbreakdown (a fraction of E_k) field is applied to the air, the number densities of electrons and O^- ions exponentially increase with a rate slightly smaller than the electron impact ionization rate at this field [*Liu*, 2012]. Since the electron impact ionization rate increases rapidly with the electric field and typical conventional streamer head fields are about 3–5E_k, the ionization rate at a subbreakdown field of a fraction of E_k is not fast enough to initiate the conventional streamer [*Liu*, 2012]. When the three-body attachment becomes more important at lower dense atmosphere, the electrons are mainly converted to O_2^- ions, the electron detachment of which is much slower, and the ionization degree growth at a subbreakdown field is less significant.

[55] On the other hand, measurements of thundercloud electric fields have consistently given maximum values about an order of magnitude smaller than E_k [e.g., *Stolzenburg et al.*, 2007]. To circumvent the problem of having the thundercloud field exceed E_k for lightning initiation, the theory that conventional streamers can be initiated in the region around hydrometeors (water droplets or ice particles), where the thundercloud field is greatly amplified was brought forward. Streamer simulations reported in *Liu et al.* [2012] indicated that the conventional positive streamers are indeed able to form from small ionization columns in an electric field of 0.5E_k. Since both water and ice have a very large dielectric constant, hydrometeors can amplify the external field as much as the conducting objects. In addition, because electron avalanches in the enhanced field region move toward the tips of the hydrometeors or the columns where the positive streamers are initiated, the positive streamer formation around the hydrometeors should also be similar to the case from the ionization column. Simulations also showed possible initiation of the streamers from the ionization column at one third of E_k, although the streamers tend to branch during the formation [*Sadighi et al.*, 2011]. The sizes of the ionization columns used in the simulations are close to the measured sizes of thundercloud hydrometeors [*Sadighi et al.*, 2011].

[56] Relativistic feedback discharges might provide additional amplification of the thundercloud field to initiate the conventional streamers in thunderclouds [e.g., *Dwyer*, 2005; *Petersen et al.*, 2008; *Babich et al.*, 2012]. *Dwyer* [2005, 2012] showed that the head field of the relativistic feedback streamer can reach E_k/3 and suggested that the conventional streamers can be initiated if hydrometeors are present there. The simulation results presented in section 3.2 verify that the peak field magnitudes can reach E_k/3–E_k/2. In particular, the results on the relativistic feedback streamer propagating in a uniform electric field further show that the head field is increasing during its propagation, while the results on the nonuniform field case show the head field is greater than 0.5E_k when the relativistic feedback streamer just enters the low-field region. Given the recent streamer modeling results discussed above, the head fields of the relativistic feedback streamers seem to be sufficient for the streamer initiation from the thundercloud hydrometeors in these fields. Another question that needs to be considered during the propagation of the feedback streamers is whether the strong head fields reside in a region long enough so that the hydrometeors there can reach steady state polarization, i.e., the permittivities of the hydrometeors reach their static values. The dielectric relaxation time of liquid water is very short, on the order of tens of picoseconds [*Raju*, 2003, p. 118], and this is also true for supercooled water down to 252 K [*Bertolini et al.*, 1982]. The relaxation time for ice is much longer, varying from 20 to 150 μs when temperature decreases from 273 to 253 K [*Gränicher et al.*, 1957]. Taking the spatial widths of the high field regions of the relativistic streamers as 100 m and their speeds as 5×10^5 m/s, the residence time of the high field is 200 μs. In addition, the formation of the streamers from the hydrometeors takes only a few tens of nanoseconds [*Sadighi et al.*, 2011; *Liu et al.*, 2012]. Therefore, the conventional streamers can definitely be initiated from the hydrometeors with proper sizes that are present in the heads of the relativistic feedback streamers. Since the dielectric relaxation time of water is much shorter than that of ice, water droplets, even if they are at supercooled temperatures, have a great advantage than the ice particles for this process.

[57] After formation of a conventional streamer, the next step for lightning initiation is the streamer-to-leader transition. The modeling work by *Riousset et al.* [2010] obtained the required time for streamer-to-spark transition in short discharge gaps that decreases from 1–2 μs to 50 ns at ground pressure for a constant reduced streamer channel field in a range of 18–28 $\times 10^5$ V/m. They further found that the transition time approximately varies as 1/n. For thundercloud altitudes, the transition time is therefore about 4–8 μs for an electric field of $E/n = 18 \times 10^5$ V/m = 0.56E_k. The electric field in the streamer channel immediately following the head of the conventional streamer is typically smaller than the applied field [*Liu et al.*, 2012], suggesting that this field for the conventional streamer initiated from hydrometeors in the feedback streamer head is at most E_k/3–E_k/2. However, as shown in *Liu* [2010], the conventional streamer draws an exponentially increasing current when it propagates in an electric field greater than its stable propagation threshold field (about E_k/7 for positive streamers). This results in an increase in the electric field in the channel far behind the conventional streamer head, which is the physical mechanism driving the observed luminous sprite streamer trails [*Liu*, 2010; *Kosar et al.*, 2012]. The increasing rate of the channel field depends on the ambient field, and the resulting channel field can be even greater than E_k [*Liu*, 2010; *Kosar et al*., 2012]. Therefore, the streamer-to-leader transition time for the conventional streamer initiated from the feedback streamer head is expected on the order of microseconds. More recently, *da Silva and Pasko* [2012] have developed a new model that takes into account the contraction of a gas channel conducting a current as well as other processes included in the work of *Riousset et al.* [2010]. This model may be more accurate for studying streamer-to-leader transition [*da Silva and Pasko*, 2012]. Their results indicate that given an external current of 2 A (e.g., the current drawn by the streamer coronas), the transition time is about 10 μs at 11 km altitude. If the current increases to 10 A, the time is further reduced to about 1 μs.

[58] It seems that leaders can be initiated from the feedback streamer head too, since the 200 μs residence time of the feedback streamer head is long enough for the sequence

of the following events: hydrometeors reaching steady state polarization, streamers forming from the polarized hydrometeors, and leaders originating from the streamers. It should be noted that in the above discussion for the streamer initiation from the hydrometeor in the feedback streamer head, the hydrometeor can as well be replaced by localized conductivity enhancements in the feedback streamer head, which might be produced due to some existing inhomogeneities in its path, breaking of the feedback streamer head, etc.

5. Summary and Conclusions

[59] The results reported in this paper can be summarized as follows.

[60] 1. This study confirms all the aspects of the work by *Dwyer* [2012]. Most importantly and generally, intense gamma ray flashes can be produced naturally by the relativistic feedback discharge developing in large-scale thundercloud and lightning fields with magnitudes reported from measurements.

[61] 2. The modeling results indicate that the durations of TGF pulses produced by relativistic feedback discharges vary from tens of microseconds to several milliseconds. Millisecond long TGF pulses can be produced by a self-propagating relativistic feedback streamer during its continuous propagation.

[62] 3. Typical relativistic feedback streamers propagate in a pulsed manner initially and continuously at a later stage. The head electric field of the streamer can reach one third to half of the conventional breakdown threshold field, which results in an ion density of 3–10 $\times 10^{14}$ m^{-3} in the streamer head. The spatial widths of the streamer head field are about 100 m and the streamer speed is about 5×10^5 m/s.

[63] 4. Conventional positive streamers can be initiated from thundercloud hydrometeors or inhomogeneities of enhanced conductivities of millimeter sizes if they are present in the relativistic feedback streamer heads. The positive streamers may further result in formation of leaders.

[64] **Acknowledgments.** This research was supported in part by NSF grants ATM 0838867 and ATM 0955379 and a DARPA grant HR0011-1-10-1- 0061. We wish to thank Hamid Rassoul and Eric Cramer for very useful discussions.

References

Albert, J. M., and S. L. Young (2005), Multidimensional quasi-linear diffusion of radiation belt electrons, *Geophys. Res. Lett.*, *32*, L14110, doi:10.1029/2005GL023191.

Babich, L. P., E. I. Bochkov, J. R. Dwyer, and I. M. Kutsyk (2012), Numerical simulations of local thundercloud field enhancements caused by runaway avalanches seeded by cosmic rays and their role in lightning initiation, *J. Geophys. Res.*, *117*, A09316, doi:10.1029/2012JA017799.

Bertolini, D., M. Cassettari, and G. Salvetti (1982), The dielectric relaxation time of supercooled water, *J. Chem. Phys.*, *76*, 3285–3290, doi:10.1063/1.443323.

Briggs, M. S., et al. (2010), First results on terrestrial gamma ray flashes from the Fermi Gamma-ray Burst Monitor, *J. Geophys. Res.*, *115*(A14), A07323, doi:10.1029/2009JA015242.

Briggs, M. S., et al. (2011), Electron-positron beams from terrestrial lightning observed with Fermi GBM, *Geophys. Res. Lett.*, *38*, L02808, doi:10.1029/2010GL046259.

Carlson, B. E., N. G. Lehtinen, and U. S. Inan (2007), Constraints on terrestrial gamma ray flash production from satellite observation, *Geophys. Res. Lett.*, *34*, L08809, doi:10.1029/2006GL029229.

Carlson, B. E., N. G. Lehtinen, and U. S. Inan (2009), Observations of terrestrial gamma-ray flash electrons, *AIP Conference Proceedings*, *1118*(1), 84–91, doi:10.1063/1.3137717.

Celestin, S., and V. P. Pasko (2011), Energy and fluxes of thermal runaway electrons produced by exponential growth of streamers during the stepping of lightning leaders and in transient luminous events, *J. Geophys. Res.*, *116*(A15), A03315, doi:10.1029/2010JA016260.

Celestin, S., W. Xu, and V. P. Pasko (2012), Terrestrial gamma ray flashes with energies up to 100 MeV produced by nonequilibrium acceleration of electrons in lightning, *J. Geophys. Res.*, *117*(A16), A05315, doi:10.1029/2012JA017535.

Chanrion, O., and T. Neubert (2008), A PIC-MCC code for simulation of streamer propagation in air, *J. Comput. Phys.*, *227*, 7222–7245, doi:10.1016/j.jcp.2008.04.016.

Chanrion, O., and T. Neubert (2010), Production of runaway electrons by negative streamer discharges, *J. Geophys. Res.*, *115*(A14), A00E32, doi:10.1029/2009JA014774.

Cohen, M. B., U. S. Inan, and G. Fishman (2006), Terrestrial gamma ray flashes observed aboard the Compton Gamma Ray Observatory/Burst and Transient Source Experiment and ELF/VLF radio atmospherics, *J. Geophys. Res.*, *111*, D24109, doi:10.1029/2005JD006987.

Cohen, M. B., U. S. Inan, R. K. Said, M. S. Briggs, G. J. Fishman, V. Connaughton, and S. A. Cummer (2010a), A lightning discharge producing a beam of relativistic electrons into space, *Geophys. Res. Lett.*, *37*, L18806, doi:10.1029/2010GL044481.

Cohen, M. B., U. S. Inan, R. K. Said, and T. Gjestland (2010b), Geolocation of terrestrial gamma-ray flash source lightning, *Geophys. Res. Lett.*, *37*, L02801, doi:10.1029/2009GL041753.

Connaughton, V., et al. (2010), Associations between Fermi Gamma-ray Burst Monitor terrestrial gamma ray flashes and sferics from the World Wide Lightning Location Network, *J. Geophys. Res.*, *115*(A14), A12307, doi:10.1029/2010JA015681.

Cummer, S. A., Y. Zhai, W. Hu, D. M. Smith, L. I. Lopez, and M. A. Stanley (2005), Measurements and implications of the relationship between lightning and terrestrial gamma ray flashes, *Geophys. Res. Lett.*, *32*, L08811, doi:10.1029/2005GL022778.

Cummer, S. A., G. Lu, M. S. Briggs, V. Connaughton, S. Xiong, G. J. Fishman, and J. R. Dwyer (2011), The lightning-TGF relationship on microsecond timescales, *Geophys. Res. Lett.*, *38*, L14810, doi:10.1029/2011GL048099.

da Silva, C. L., and V. P. Pasko (2012), Simulation of leader speeds at gigantic jet altitudes, *Geophys. Res. Lett.*, *39*, L13805, doi:10.1029/2012GL052251.

Dwyer, J. R. (2003), A fundamental limit on electric fields in air, *Geophys. Res. Lett.*, *30*(20), 2055, doi:10.1029/2003GL017781.

Dwyer, J. R. (2005), The initiation of lightning by runaway air breakdown, *Geophys. Res. Lett.*, *32*(20), L20808, doi:10.1029/2005GL023975.

Dwyer, J. R. (2008), Source mechanisms of terrestrial gamma-ray flashes, *J. Geophys. Res.*, *113*(D10), D10103, doi:10.1029/2007JD009248.

Dwyer, J. R. (2010), Diffusion of relativistic runaway electrons and implications for lightning initiation, *J. Geophys. Res.*, *115*(D10), A00E14, doi:10.1029/2009JA014504.

Dwyer, J. R. (2012), The relativistic feedback discharge model of terrestrial gamma ray flashes, *J. Geophys. Res.*, *117*, A02308, doi:10.1029/2011JA017160.

Dwyer, J. R., and L. P. Babich (2011), Low-energy electron production by relativistic runaway electron avalanches in air, *J. Geophys. Res.*, *116*(A15), A09301, doi:10.1029/2011JA016494.

Dwyer, J. R., and D. M. Smith (2005), A comparison between Monte carlo simulations of runaway breakdown and terrestrial gamma-ray flash observations, *Geophys. Res. Lett.*, *32*, L22804, doi:10.1029/2005GL023848.

Dwyer, J. R., et al. (2003), Energetic radiation during rocket-triggered lightning, *Science*, *299*(5607), 694–697, doi:10.1126/science.1078940.

Dwyer, J. R., et al. (2005), X-ray bursts associated with leader steps in cloud-to-ground lightning, *Geophys. Res. Lett.*, *32*, L01803, doi:10.1029/2004GL021782.

Dwyer, J. R., B. W. Grefenstette, and D. M. Smith (2008), High-energy electron beams launched into space by thunderstorms, *Geophys. Res. Lett.*, *35*, L02815, doi:10.1029/2007GL032430.

Dwyer, J. R., D. M. Smith, M. A. Uman, Z. Saleh, B. Grefenstette, B. Hazelton, and H. K. Rassoul (2010), Estimation of the fluence of high-energy electron bursts produced by thunderclouds and the resulting radiation doses received in aircraft, *J. Geophys. Res.*, *115*, D09206, doi:10.1029/2009JD012039.

Dwyer, J. R., D. M. Smith, and S. A. Cummer (2012), High-energy atmospheric physics: Terrestrial gamma-ray flashes and related phenomena, *Space Sci. Rev.* doi:10.1007/s11214-012-9894-0

Fishman, G. J., et al. (1994), Discovery of intense gamma-ray flashes of atmospheric origin, *Science*, *264*(5163), 1313

Fishman, G. J., et al. (2011), Temporal properties of the terrestrial gamma-ray flashes from the Gamma-Ray Burst Monitor on the

Fermi Observatory, *J. Geophys. Res.*, *116*(A15), A07304, doi:10.1029/2010JA016084.

Gordillo-Vázquez, F. J. (2008), Air plasma kinetics under the influence of sprites, *J. Phys. D: Appl. Phys.*, *41*(23), 234016, doi:10.1088/0022-3727/41/23/234016.

Gränicher, H., C. Jaccard, P. Scherrer, and A. Steinemann (1957), Dielectric relaxation and the electrical conductivity of ice crystals, *Discuss. Faraday Soc.*, *23*, 50–62, doi:10.1039/DF9572300050.

Grefenstette, B. W., D. M. Smith, B. J. Hazelton, and L. I. Lopez (2009), First RHESSI terrestrial gamma ray flash catalog, *J. Geophys. Res.*, *114*, A02314, doi:10.1029/2008JA013721.

Gurevich, A. V. (1961), On the theory of runaway electrons, *Sov. Phys. JETP*, *12*, 904–912

Gurevich, A. V., G. M. Milikh, and R. A. Roussel-Dupré (1992), Runaway electron mechanism of air breakdown and preconditioning during a thunderstorm, *Phys. Lett. A.*, *165*(5-6), 463–468, doi:10.1016/0375-9601(92)90348-P.

Inan, U. S., S. C. Reising, G. J. Fishman, and J. M. Horack (1996), On the association of terrestrial gamma-ray bursts with lightning and implications for sprites, *Geophys. Res. Lett.*, *23*(9), 1017–1020.

Kosar, B. C., N. Y. Liu, and H. K. Rassoul (2012), Luminosity and propagation characteristics of sprite streamers initiated from small ionospheric disturbances at subbreakdown conditions, *J. Geophys. Res.*, *117*(A16), A08328, doi:10.1029/2012JA017632.

Kulikovsky, A. A. (1995), A more accurate Scharfetter-Gummel algorithm of electron transport for semiconductor and gas discharge simulation, *J. Comput. Phys.*, *119*, 149–155.

LeVeque, R. J. (2002), *Finite Volume Methods for Hyperbolic Problems*, Cambridge University Press, New York.

Li, C., U. Ebert, W. J. M. Brok, and W. Hundsdorfer (2008), FAST TRACK COMMUNICATION: Spatial coupling of particle and fluid models for streamers: Where nonlocality matters, *J. Phys. D: Appl. Phys.*, *41*(3), 032,005, doi:10.1088/0022-3727/41/3/032005.

Liu, N. Y. (2010), Model of sprite luminous trail caused by increasing streamer current, *Geophys. Res. Lett.*, *37*, L04102, doi:10.1029/2009GL042214.

Liu, N. Y. (2012), Multiple ion species fluid modeling of sprite halos and the role of electron detachment of O^- in their dynamics, *J. Geophys. Res.*, *117*, A03308, doi:10.1029/2011JA017062.

Liu, N. Y., and V. P. Pasko (2004), Effects of photoionization on propagation and branching of positive and negative streamers in sprites, *J. Geophys. Res.*, *109*, A04301, doi:10.1029/2003JA010064.

Liu, N. Y., and V. P. Pasko (2006), Effects of photoionization on similarity properties of streamers at various pressures in air, *J. Phys. D: Appl. Phys.*, *39*, 327–334, doi:10.1088/0022-3727/39/2/013.

Liu, N. Y., and D. D. Sentman (2010), A modeling study of sprite streamer chemistry, *Abstract AE13B-04 Presented at 2010 Fall Meeting,* AGU, San Francisco, Calif., 13-17 Dec.

Liu, N. Y., V. P. Pasko, K. Adams, H. C. Stenbaek-Nielsen, and M. McHarg (2009a), Comparison of acceleration, expansion and brightness of sprite streamers obtained from modeling and high-speed video observations, *J. Geophys. Res.*, *114*, A00E03, doi:10.1029/2008JA013720.

Liu, N. Y., V. P. Pasko, H. U. Frey, S. B. Mende, H.-T. Su, A. B. Chen, R.-R. Hsu, and L.-C. Lee (2009b), Assessment of sprite initiating electric fields and quenching altitude of $a^1\Pi_g$ state of N_2 using sprite streamer modeling and ISUAL spectrophotometric measurements, *J. Geophys. Res.*, *114*, A00E02, doi:10.1029/2008JA013735.

Liu, N. Y., B. Kosar, S. Sadighi, J. R. Dwyer, and H. K. Rassoul (2012), Formation of streamer discharges from an isolated ionization column at subbreakdown conditions, *Phys. Rev. Lett.*, *109*(2), 025002, doi:10.1103/PhysRevLett.109.025002.

Lu, G., R. J. Blakeslee, J. Li, D. M. Smith, X.-M. Shao, E. W. McCaul, D. E. Buechler, H. J. Christian, J. M. Hall, and S. A. Cummer (2010), Lightning mapping observation of a terrestrial gamma-ray flash, *Geophys. Res. Lett.*, *37*, L11806, doi:10.1029/2010GL043494.

Lu, G., S. A. Cummer, J. Li, F. Han, D. M. Smith, and B. W. Grefenstette (2011), Characteristics of broadband lightning emissions associated with terrestrial gamma ray flashes, *J. Geophys. Res.*, *116*(A15), A03316, doi:10.1029/2010JA016141.

Luque, A., and F. J. Gordillo-Vázquez (2011), Mesospheric electric breakdown and delayed sprite ignition caused by electron detachment, *Nat. Geosci.*, *5*, 22–25, doi:10.1038/ngeo1314.

Marisaldi, M., et al. (2010), Detection of terrestrial gamma ray flashes up to 40 MeV by the AGILE satellite, *J. Geophys. Res.*, *115*(A14), A00E13, doi:10.1029/2009JA014502.

Moore, C. B., K. B. Eack, G. D. Aulich, and W. Rison (2001), Energetic radiation associated with lightning stepped-leaders, *Geophys. Res. Lett.*, *28*(11), 2141–2144, doi:10.1029/2001GL013140.

Moss, G. D., V. P. Pasko, N. Liu, and G. Veronis (2006), Monte Carlo model for analysis of thermal runaway electrons in streamer tips in transient luminous events and streamer zones of lightning leaders, *J. Geophys. Res.*, *111*, A02307, doi:10.1029/2005JA011350.

Petersen, D., M. Bailey, W. H. Beasley, and J. Hallett (2008), A brief review of the problem of lightning initiation and a hypothesis of initial lightning leader formation, *J. Geophys. Res.*, *113*, D17205, doi:10.1029/2007JD009036.

Press, W. H., B. P. Flannery, S. A. Teukolsky, and W. T. Vetterling (1992), *Numerical Recipes in C: The Art of Scientific Computing* second ed., Cambridge Univ. Press, New York, NY.

Raizer, Y. P. (1991), *Gas Discharge Physics*, Springer-Verlag, New York.

Raju, G. G. (2003), *Dielectrics in Electric Fields*, Marcel Dekker, New York.

Riousset, J. A., V. P. Pasko, and A. Bourdon (2010), Air-density-dependent model for analysis of air heating associated with streamers, leaders, and transient luminous events, *J. Geophys. Res.*, *115*, A12321, doi:10.1029/2010JA015918.

Sadighi, S., N. Y. Liu, J. R. Dwyer, and H. K. Rassoul (2011), Streamer initiation from hydrometeors in weak thundercloud electric fields, *Abstract AE31A-0271 Presented at 2011 Fall Meeting* AGU, San Francisco, Calif., 5-9 Dec.

Shao, X.-M., T. Hamlin, and D. M. Smith (2010), A closer examination of terrestrial gamma-ray flash-related lightning processes, *J. Geophys. Res.*, *115*(A14), A00E30, doi:10.1029/2009JA014835.

Smith, D. M., L. I. Lopez, R. P. Lin, and C. P. Barrington-Leigh (2005), Terrestrial gamma-ray flashes observed up to 20 MeV, *Science*, *307*(5712), 1085–1088, doi:10.1126/science.1107466.

Stanley, M. A., X.-M. Shao, D. M. Smith, L. I. Lopez, M. B. Pongratz, J. D. Harlin, M. Stock, and A. Regan (2006), A link between terrestrial gamma-ray flashes and intracloud lightning discharges, *Geophys. Res. Lett.*, *33*, L06803, doi:10.1029/2005GL025537.

Stolzenburg, M., and T. C. Marshall (2008), Serial profiles of electrostatic potential in five New Mexico thunderstorms, *J. Geophys. Res.*, *113*(D13), doi:10.1029/2007JD009495.

Stolzenburg, M., T. C. Marshall, W. D. Rust, E. Bruning, D. R. MacGorman, and T. Hamlin (2007), Electric field values observed near lightning flash initiations, *Geophys. Res. Lett.*, *34*(4), L04804, doi:10.1029/2006GL028777.

Symbalisty, E. M. D., R. A. Roussel-Dupre, and V. A. Yukhimuk (1998), Finite volume solution of the relativistic Boltzmann equation for electron avalanche studies, *IEEE Trans. Plasma Sci.*, *26*(5), 1575–1582, doi:10.1109/27.736065.

Tavani, M., et al. (2011), Terrestrial gamma-ray flashes as powerful particle accelerators, *Phys. Rev. Lett.*, *106*(1), 018501, doi:10.1103/PhysRevLett.106.018501.

Wilson, C. T. R. (1925), The acceleration of β-particles in strong electric fields such as those in thunderclouds, *Proc. Cambridge Philos. Soc.*, *22*, 534–538